JGR Earth Surface

RESEARCH ARTICLE

10.1029/2020JF005619

Rockwall Slope Erosion in the Northwestern Himalaya

Elizabeth N. Orr[1], Lewis A. Owen[2], Sourav Saha[3], Sarah J. Hammer[4], and Marc W. Caffee[5,6]

[1]GFZ German Research Centre for Geosciences, Potsdam, Germany, [2]Department of Marine, Earth, and Atmospheric Sciences, North Carolina State University, Raleigh, NC, USA, [3]Department of Earth, Planetary, and Space Sciences, University of California, Los Angeles, CA, USA, [4]Department of Geology, University of Cincinnati, Cincinnati, OH, USA, [5]Department of Physics, Purdue University, West Lafayette, IN, USA, [6]Department of Earth, Atmospheric and Planetary Sciences, Purdue University, West Lafayette, IN, USA

Key Points:

- Rates of periglacial rockwall slope erosion are defined for the northwestern Himalaya using cosmogenic ^{10}Be concentrations in sediment from medial moraines
- Tectonically driven uplift offers a first-order control on patterns of rockwall slope erosion
- Precipitation and temperature play secondary roles in this erosion

Correspondence to:

E. N. Orr,
elizabeth.orr@gfz-potsdam.de

Citation:

Orr, E. N., Owen, L. A., Saha, S., Hammer, S. J., & Caffee, M. W. (2021). Rockwall slope erosion in the northwestern Himalaya. *Journal of Geophysical Research: Earth Surface*, *126*, e2020JF005619. https://doi.org/10.1029/2020JF005619

Received 18 MAR 2020
Accepted 12 NOV 2020

Abstract Rockwall slope erosion is an important component of alpine landscape evolution, yet the role of climate and tectonics in driving this erosion remains unclear. We define the distribution and magnitude of periglacial rockwall slope erosion across 12 catchments in Himachal Pradesh and Jammu and Kashmir in the Himalaya of northern India using cosmogenic ^{10}Be concentrations in sediment from medial moraines. Beryllium-10 concentrations range from $0.5 \pm 0.04 \times 10^4$ to $260.0 \pm 12.5 \times 10^4$ at/g SiO_2, which yield erosion rates between 7.6 ± 1.0 and 0.02 ± 0.004 mm/a. Between ~0.02 and ~8 m of rockwall slope erosion would be possible in this setting across a single millennium, and >2 km when extrapolated for the Quaternary period. This erosion affects catchment sediment flux and glacier dynamics, and helps to establish the pace of topographic change at the headwaters of catchments. We combine rockwall erosion records from the Himalaya of Himachal Pradesh, Jammu and Kashmir, and Uttarakhand in India and Baltistan in Pakistan to create a regional erosion data set. Rockwall slope erosion rates progressively decrease with distance north from the Main Central Thrust and into the interior of the orogen. The distribution and magnitude of this erosion is most closely associated with records of Himalayan denudation and rock uplift, where the highest rates of change are recorded in the Greater Himalaya sequences. This suggests that tectonically driven uplift, rather than climate, is a first order control on patterns of rockwall slope erosion in the northwestern Himalaya. Precipitation and temperature would therefore come as secondary controls.

1. Introduction

A number of studies have underlined the importance of the erosion of bedrock-dominated slopes, referred to here as rockwall slopes (Figure 1), in catchment sediment flux, relief production, topographic configuration, and glacier dynamics of steep alpine environments (Benn et al., 2012; Heimsath & McGlynn, 2008; MacGregor et al., 2009; Orr et al., 2019; Scherler & Egholm, 2020; Seong et al., 2009; Ward & Anderson, 2011). The lateral erosion of slopes has been shown to exceed rates of vertical incision through glacial and fluvial processes, and therefore to a greater extent than previously thought, contribute to denudation budgets and landscape change on the catchment and mountain range scale (Brocklehurst & Whipple, 2006; Foster et al., 2008).

The erosion or destabilization of rockwalls is commonly attributed to climate-modulated processes (Böhlert et al., 2008; Hales & Roering, 2005; Krautblatter & Moore, 2014). Changes to slope hydrology and weathering environments, permafrost degradation, and stress redistribution from changing glacier extents and the (un)loading of slopes through deposition and erosion can each decrease slope stability and lead to mass wasting (André, 2003; Cossart et al., 2008; Gallach et al., 2018; McColl, 2012). Periglacial weathering processes that are driven by moisture and temperature variability, and include freeze-thaw, frost cracking and ice wedging, are particularly critical for the detachment and disintegration of rock from rockwalls (Eppes & Keanini, 2017; Heimsath & McGlynn, 2008; McColl & Davies, 2013). This detachment is considered stochastic, and through rockfall and other mass wasting delivers debris to glacier surfaces (Gibson et al., 2017; Sanders et al., 2012; Sarr et al., 2019).

Rockwall erosion is also sensitive to the lithology and structure of the bedrock slope, glacial/fluvial erosion, and seismicity (Leith et al., 2010; Sanchez et al., 2009). Disentangling climatic and non-climatic controls of slope failure and longer-term rockwall slope evolution is challenging, with several studies arguing that a

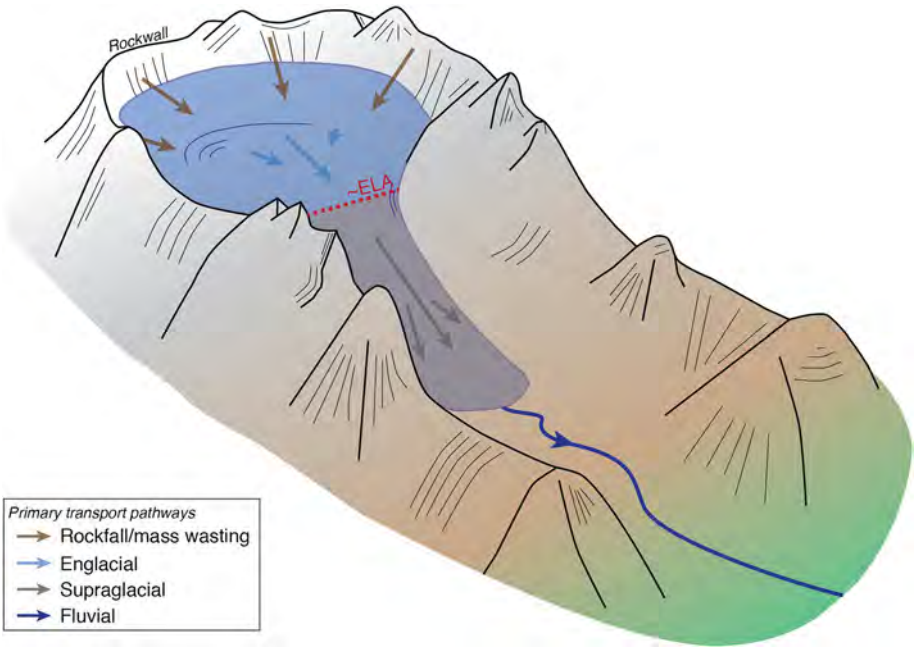

Figure 1. Schematic diagram of glaciated catchment with primary debris transport pathways . The rockwall is defined for this study as the headwater bedrock slopes above the ELA of each glacier. This study focuses on erosion via periglacial processes only. The medial moraines and supraglacial debris are revealed below the ELA (gray shading). ELA, equilibrium-line altitude.

combination of factors instead dictates the stability of steep rockwalls in alpine regions (Gallach et al., 2018; Krautblatter & Moore, 2014; McColl, 2012).

Orr et al. (2019) were able to identify a tentative positive relationship between periglacial rockwall slope erosion and precipitation in the northwestern (NW) Himalaya by comparing erosion rates inferred from cosmogenic nuclide concentrations of medial moraine sediment across three glacier systems. Higher rates of erosion were determined for catchments with enhanced monsoon precipitation. Rather, than identifying precipitation as the only control, their study instead suggests that rockwall slope erosion is more complex, and is likely dictated by the interaction between tectonics, climate, topography, and surface processes that are specific to each catchment. This challenges the argument that in the tectonically active ranges of the Himalaya, the rate of debris transfer from the hillslope to the glacier surface is largely controlled by rock uplift and topographic steepness (Gibson et al., 2017; Scherler et al., 2011).

In this study, we seek to better define the distribution and magnitude of periglacial rockwall slope erosion in the NW Himalaya by building upon the work of Orr et al. (2019) and quantifying erosion rates for a suite of 12 catchments. Rates of rockwall slope erosion are derived from cosmogenic nuclide ^{10}Be concentrations measured in sediment from medial moraines. Our new erosion data set is combined with existing rockwall slope erosion records from Seong et al. (2009), Scherler and Egholm (2020), and Orr et al. (2019). This regional rockwall erosion data set is compared to records of catchment-wide erosion and exhumation for the NW Himalaya to evaluate the extent to which rockwall slope erosion may differ from other records of landscape change, which have been averaged across various spatial and temporal scales. We compare patterns of rockwall slope erosion to variations in geology, tectonics, climate and topography throughout the region, to resolve the primary controls of rockwall slope erosion in the NW Himalaya. Steep north-south gradients in elevation, slope, relief, rock uplift, and precipitation has made the Himalayan-Tibetan orogen an ideal location to evaluate these controls (Bookhagen & Burbank, 2006, 2010; Scherler et al., 2011). In line with existing assessments of the principle controls of rockwall slope erosion in alpine settings (Böhlert et al., 2008; Hales & Roering, 2005; Krautblatter & Moore, 2014), and landscape change more generally throughout the orogen (Clift et al., 2008; Deeken et al., 2011; Gabet et al., 2008; Grujic et al., 2006; Thiede et al., 2004; Wulf et al., 2010), our hypothesis is that climate-modulated processes will largely dictate the patterns of

rockwall slope erosion in the NW Himalaya. Finally, we determine to what extent rockwall slope erosion and its controls, in this high-altitude and high relief setting, can contribute to the longstanding debate over the significance of climate versus tectonics in driving both short- and long-term landscape change. Until now, much of the research that has contributed to this debate is based in either unglaciated or deglaciated environments. This study will provide a unique insight into how erosional processes modulated by climate and/or tectonics operate within glaciated catchment headwaters.

1.1. Regional Setting

The Himalayan-Tibetan orogen is the result of the continued continental collision and partial subduction between the Indian and Eurasian lithospheric plates (Searle et al., 1997). The Indus-Tsangpo Suture Zone (ITSZ) defines the collision zone between these plates in the NW Himalaya and contains remnants of the Neo-Tethys Ocean (Figure 2). The suture zone marks the northern boundary of the Tethyan Himalaya (Schlup et al., 2003; M. Searle, 1986; Steck et al., 1998). Between the early Miocene and Pleistocene, deformation driven crustal shortening initiated the development of a sequence of foreland propagating thrust systems that divide the lithotectonic units that lie south of the Tethyan Himalaya. The South-Tibetan Detachment (STD) and the Main Central Thrust (MCT) bound the Greater Himalaya Crystalline Core Zone to the north and south, respectively (Frank et al., 1973; Miller et al., 2001; Searle & Fryer, 1986; Vannay et al., 2004; Walker et al., 1999). This unit has been divided into two subunits: southern Greater Himalaya sequence (GHS-S) and northern Greater Himalaya sequence (GHS-N; DeCelles et al., 2001; Thiede & Ehlers, 2013). South of the Greater Himalaya and MCT lies the Lesser Himalaya sequence, which is bounded to the south by the Main Boundary Thrust (MBT). South of the MBT lies the Sub-Himalaya and Main Frontal Thrust (MFT; Upreti, 1999; Miller et al., 2000; Vannay et al., 2004). Continued crustal shortening and thrust and strike-slip faulting throughout the orogen means that the NW Himalaya remains tectonically active (Bojar et al., 2005; Hodges et al., 2004; Vannay et al., 2004), even though some regions in northern India, such as Ladakh, have undergone tectonic quiescence or dormancy since the early Miocene (Kristein et al., 2006, 2009). Hodges (2000), Yin and Harrison (2000), and Streule et al. (2010) provide further details of the Himalayan lithotectonic units and the timing of movement throughout the fault systems.

Two atmospheric systems primarily govern northwest Himalayan climate: the Indian summer monsoon that advects moisture from the Indian Ocean between late May and September, and the Northern Hemispheric mid-latitude westerlies, which bring moisture from the Mediterranean, Black and Caspian seas between December and March (Benn & Owen, 1998; Gadgil, 2003; Mölg et al., 2014; Lang & Barros, 2004; Wulf et al., 2010). A steep south-north precipitation gradient likely became established during the late Miocene, perpendicular to the strike of the mountain belt (~8 Ma; Liu & Dong, 2013; Qiang et al., 2001), due to the high elevation topography of the Greater Himalaya inhibiting the northward migration of moisture to the interior of the orogen. Monsoon air masses are forced to ascend, condense and form clouds along the Himalayan front, which creates a rain shadow down the leeside of this orographic barrier (Bookhagen et al., 2005a, 2005b; Wulf et al., 2010). During times of increased monsoon strength, moisture is thought to penetrate farther into the interior of the orogen (Bookhagen et al., 2005a, 2005b; Finkel et al., 2003; Wulf et al., 2010). The northern hemispheric mid-latitude westerlies operate at higher tropospheric levels than the Indian summer monsoon. The orographic capture of moisture transported by this atmospheric system is therefore focused in high elevation mountain ranges (>4,500 m asl) as winter snowfall (Lang & Barros, 2004; Weiers, 1995). Today, mean annual precipitation declines from ~1,500 to 3,000 mm in the Lesser and Greater Himalaya ranges, to <150 mm in the interior of the Tethyan Himalaya and Tibetan Plateau (Bookhagen & Burbank, 2006, Figure 2).

The distribution and magnitude of precipitation has been shown to vary both temporally and spatially throughout the Himalayan-Tibetan orogen during the late Quaternary (Bookhagen et al., 2005a, 2005b; Burbank et al., 2003). Fluctuations in monsoon strength driven by changes in orbital insolation, the migration of the intertropical convergence zone, convective localized monsoon storms, and sporadic heavy rainfall are thought to cause some of this variability (Finkel et al., 2003; Owen et al., 2008; Thomas et al., 2016). On the local to regional scale (10^{2-4} km^2), topography and wind direction exert controls on the migration of moisture throughout the NW Himalaya (Bookhagen et al., 2005a, b), and create localized microclimates throughout individual mountain ranges (Benn & Owen, 1998; Bookhagen & Burbank, 2010; Wulf

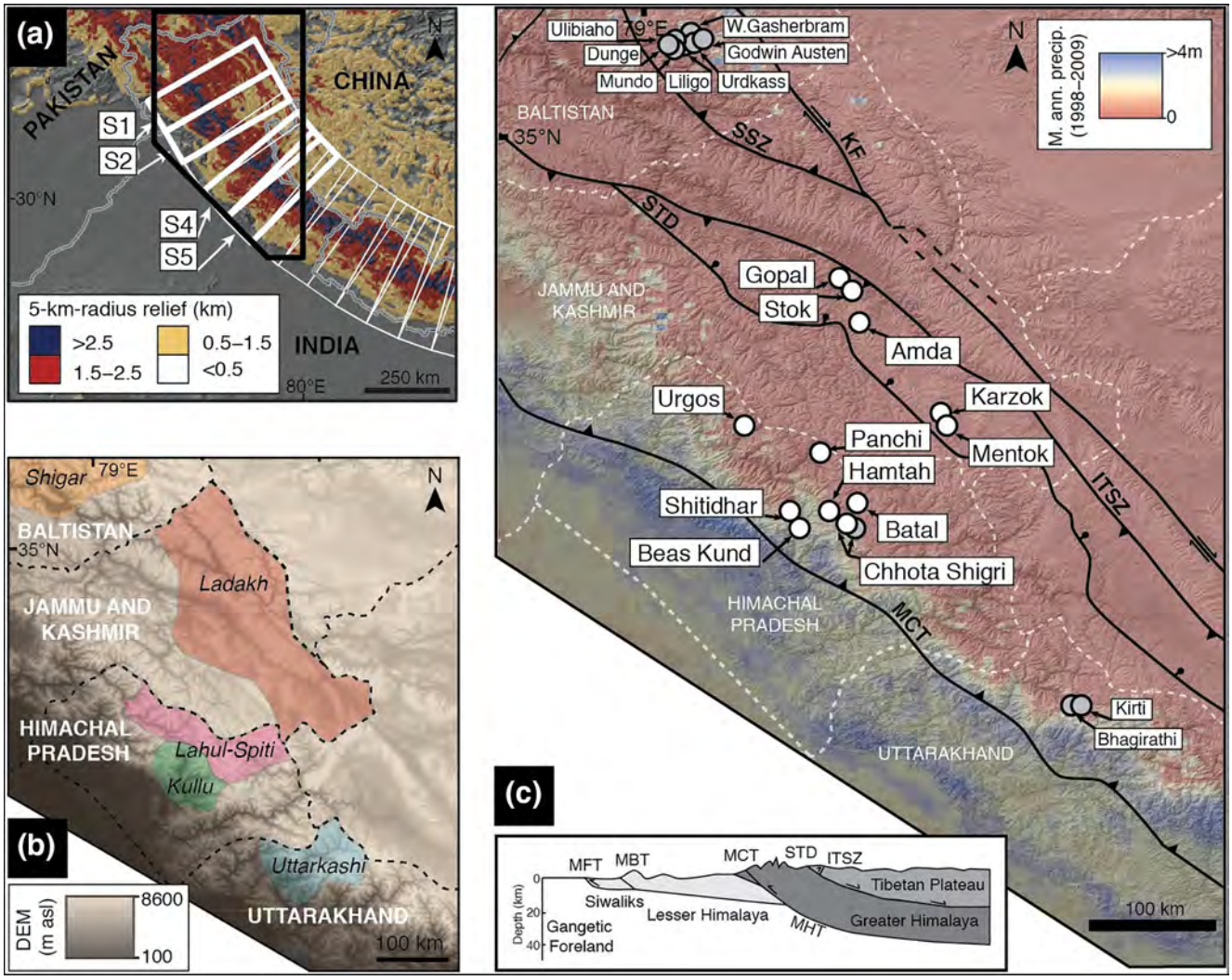

Figure 2. Overview of the study area in the northwestern (NW) Himalaya. (a) Study area location (black polygon) is outlined on a 5-km-radius relief map with swath polygons (bold polygons S1, 2, 4, 5 are referred to in Figure 7) modified from Bookhagen and Burbank (2006). A 3-km-radius relief data set is used in following analyses. (b) ASTER GDEM of study area (see a) with investigated regions and districts outlined. (c) Hillshade map of the study area is overlain by mean annual precipitation (TRMM 2B31; Bookhagen & Burbank, 2006). White circles: location of catchments of this study. Gray circles: location of published rockwall slope erosion rate studies: Baltoro glacier system (Seong et al., 2009), Chhota Shigri (Scherler & Egholm, 2020), Bhagirathi glacier system (Orr et al., 2019). Major faults from Hodges (2000) and Schlup et al. (2003). ASTER, Advanced Spaceborne Thermal Emission and Reflection Radiometer; ITSZ, Indus-Tsangpo Suture Zone; KF, Karakoram Fault; MBT, Main Boundary Thrust; MCT, Main Central Thrust; MFT, Main Frontal Thrust; MHT, Main Himalayan Thrust; SSZ, Shyok Suture Zone; STD, South Tibetan Detachment; Inset: simplified structure of the NW Himalaya, modified from Searle et al. (2011) and Schlup et al. (2011).

et al., 2010). Landscape change in the NW Himalaya is precipitation sensitive, where shifts in the availability and source of moisture is shown to initiate changes to sediment flux, hillslope processes (Bookhagen & Burbank, 2006; Bookhagen et al., 2005; Kumar et al., 2018; Sharma et al., 2017), and the timing of glaciation (Owen & Dortch, 2014; Saha et al., 2018).

Studies have shown that glaciation in the Himalayan-Tibetan orogen is largely influenced by climatic conditions including shifts in the strength or behavior of regional and/or global atmospheric and oceanic systems (Owen & Sharma 1998; Solomina et al., 2015, 2016; Saha et al., 2018; Watanabe et al., 1998). The Himalayan Holocene stages (HHs; Saha et al., 2018), Himalayan-Tibetan Holocene glacial stages (HTHS; Saha et al., 2019), semiarid western Himalayan-Tibetan orogen stages (SWHTs; Dortch et al., 2013), and monsoonal Himalayan-Tibetan stages (MOHITs; Murari et al., 2014) provide regional syntheses of the glacial records throughout the NW Himalaya (Table 1). Variability in the timing and forcing of glaciation across

Table 1
Details of the Investigated Catchments

Location[a]			Climate				Holocene glacial record	
Catchment	Latitude (°N)	Longitude (°E)	Mean annual precipe.[b, c] (m/a)	Mean annual temp[d] (°C)	Min. catch. temp.[e] (~°C)	Mean rockwall temp.[e] (~°C)	Local glacial stages[f] (ka)	Regional glacial stages[g] (ka)
				Ladakh				
Gopal	33.9865	77.4571	0.087 (<0.5)	5.6	−13.0	−10.6	MG1 (1.3 ± 0.2 ka)	HH2 (~1.8–0.9 ka)
Stok	33.9678	77.4698	0.087 (<0.5)	5.6	−11.6	−9.7	MS1 (1.2 ± 0.1 ka); MS2 (0.6 ± 0.2 ka)	HH1 (<1 ka); HH2 (~1.8–0.9 ka)
Amda	33.6836	77.5925	0.087 (<0.5)	5.6	−12.3	−9.8	MA1 (0.3 ± 0.1 ka); MA2C (0.5 ± 0.2 ka); MA3 (1.6 ± 0.3 ka)	HH1 (<1 ka); HH2 (~1.8–0.9 ka)
Karzok	32.9681	78.1779	0.087 (<0.5)	5.6	−12.3	−10.2	MG1 (2.1 ± 0.3 ka); MG2 (4.9 ± 0.3 ka)	HH3 (~2.7–1.8 ka); HH5 (~6.9–4.3 ka)
Mentok	32.9354	78.2124	0.087 (<0.5)	5.6	−13.7	−11.6	MM1 (0.7 ± 0.1 ka); MM2 (1.0 ± 0.1 ka)	HH1 (<1 ka); HH2 (~1.8–0.9 ka)
				Lahul-Spiti				
Urgos	32.8970	76.7679	0.95 (0.5–1.0)	17.9	−14.2	−6.9	–	–
Panchi	32.7287	77.3009	0.95 (<0.5)	17.9	−12.1	−5.8	–	–
Shitidhar	32.4197	77.1074	0.95 (<0.5)	17.9	−10.7	−2.0	–	–
Batal	32.3640	77.6032	0.95 (<0.5)	17.9	−12.1	−5.8	–	–
Chhota Shigri	32.2663	77.5288	0.95 (<0.5)	17.9	−12.8	−5.5	–	–
Hamtah	32.2680	77.3572	0.95 (0.5–1/0)	17.9	−12.8	−5.8	MH1 (0.2 ± 0.1 ka); MH3 (10.4 ± 0.3 ka)	HH1 (<1 ka); HH7 (~10.9–9.3 ka)
				Kullu				
Beas Kund	32.3532	77.0890	1.02 (0.5–1.0)	17.9	−14.9	−5.8	–	–

[a]Catchment coordinates taken from glacier snout. [b]Mean annual precipitation. Rainfall data from local weather stations. Leh Meteorological Station (34.18°N, 77.58°E, 3,500 m asl; CRUTEM4 1876–1990, Jones et al., 2012; Osborn & Jones, 2014): Gopal, Stok, Amda, Karzok, and Mentok. Chhota Shigri weather station (32.28°N, 77.53°E, 3,900 m asl; 1980–2005; Azam et al., 2014; Wagnon et al., 2007): Urgos, Panchi, Shitidhar, Batal, Chhota, and Hamtah. Bhuntar Observatory (1969–2012; 31.8°N, 77.1°E, 1,130 m asl; Azam et al., 2014): Beas Kund. [c](x) TRMM2B31 (1998–2009) annual rainfall data (Bookhagen & Burbank, 2010). [d]Temperature data from local weather stations. Leh Meteorological Station (34.18°N, 77.58°E, 3,500 m asl; CRUTEM4 1876–1990, Jones et al., 2012; Osborn & Jones, 2014): Gopal, Stok, Amda, Karzok, and Mentok. Chhota Shigri weather station (32.28°N, 77.53°E, 3,900 m asl; 1980–2005; Azam et al., 2014;Wagnon et al., 2007): Urgos, Panchi, Shitidhar, Batal, Chhota Shigri, Hamtah, and Beas Kund. [e]Temperatures estimated using local weather station data and an adiabatic lapse rate ($\Delta T/\Delta Z$) of 7°C/km Bashir & Rasul, 2010; Derbyshire et al., 1991; de Scally, 1997; Kattel et al., 2013, 2015; Pratap et al., 2013; Thayyen et al., 2005). [f]Local glacial stages from the northwestern end of the Himalayan-Tibetan orogen. Gopal: Saha et al. (2018); Stok: Orr et al. (2017), and Saha et al. (2018); Amda: Orr et al. (2018), and Saha et al. (2018); Karzok and Mentok: Hedrick et al. (2014) and Saha et al., (2018); Hamtah: Saha et al. (2018). [g]Regional glacial stages from Saha et al. (2018). Holocene regional glacial stages for Ladakh include SWHTS 2A (12.2 ± 0.8 ka), 1C (3.8 ± 0.6 ka), 1B (1.7 ± 0.2 ka), and 1A (0.4 ± 0.1 ka) from Dortch et al. (2013). Regional stages for Lahul-Spiti and Kullu include MOHITS 2A (12.9 ± 0.9 ka), 1K (11.4 ± 0.7 ka), 1J (10.1 ± 0.5 ka), 1I (9.1 ± 0.3 ka), 1H (8.1 ± 0.8 ka), 1G (7.7 ± 0.6 ka), 1F (5.4 ± 0.6 ka), 1E (3.5 ± 0.4 ka), 1D (2.3 ± 0.1 ka), 1C (1.5 ± 0.2 ka), 1B (0.7 ± 0.1 ka), and 1A (0.4 ± 0.1 ka) from Murari et al. (2014).

short distances (10^{1-2} km) throughout the NW Himalaya is commonly attributed to microclimatic variability and local geologic factors such as topography and glacier type (Anderson et al., 2014; Barr & Lovell, 2014; Owen & Dortch 2014).

1.2. Study Areas

We selected 12 accessible catchments along the south-north precipitation gradient of the NW Himalaya (Figures 2 and 3, Supporting information S2). Each catchment supports either a cirque or small valley glacier with distinct and well-preserved medial moraines. The northern-most sites of this study are located in the Ladakh and Zanskar Ranges of the Ladakh region in Jammu and Kashmir of northern India and the Shigar region of Baltistan in Pakistan (Figure 2). For this latter site, a pre-existing erosion data set

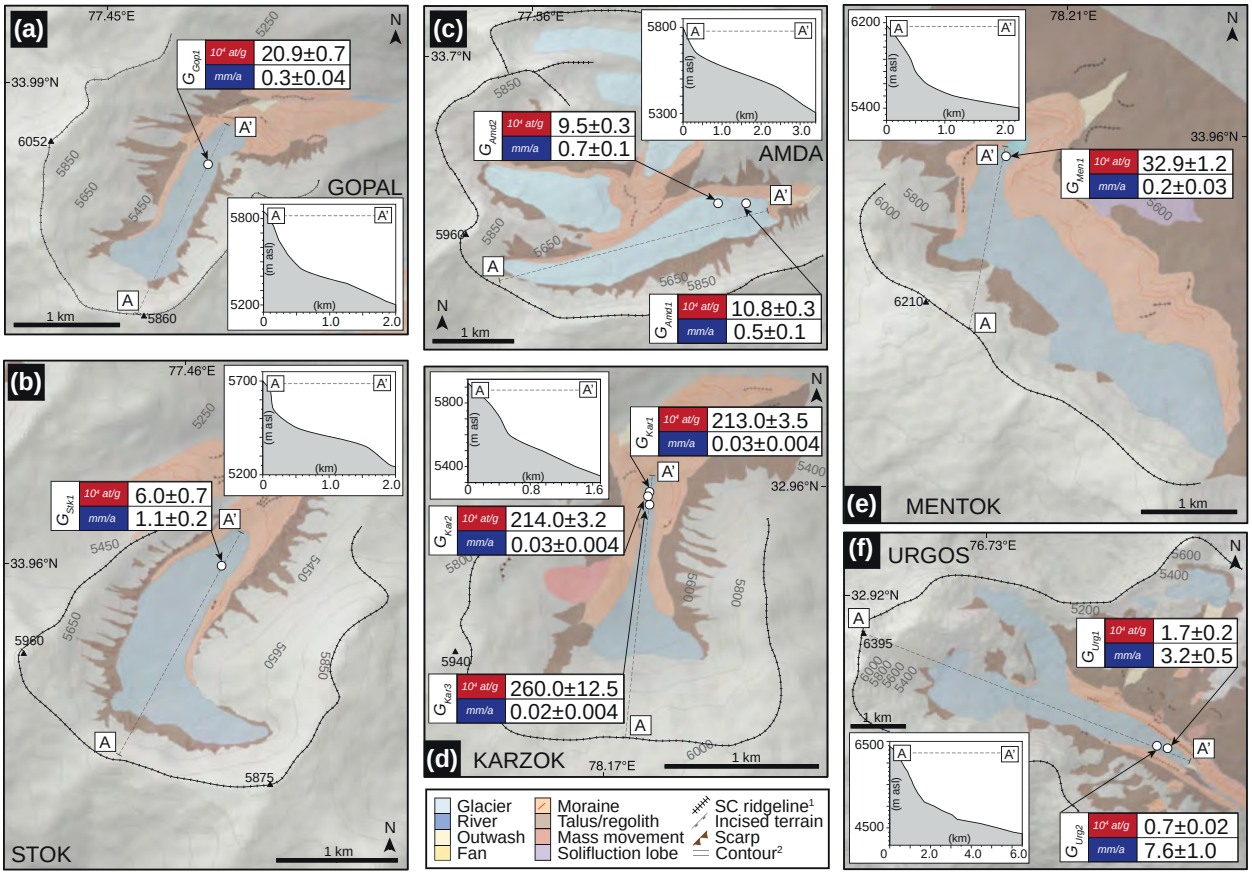

Figure 3. Geomorphic maps of the study areas including sample ^{10}Be concentrations and rockwall slope erosion rates. Inset plots: Long profile of rockwall (A- A'). (a) Gopal, (b) Stok, (c) Amda, (d) Karzok, (e) Mentok, (f) Urgos, (g) Panchi, (h) Shitidhar, (i) Batal, (j) Chhota Shigri, (k) Hamtah, (l) Beas Kund. 1: Catchment ridgeline, 2: 100-m-contour lines.

was reanalyzed. The Indian summer monsoon delivers two-thirds of the annual precipitation to Ladakh (87 mm/a; Table 1), whereas the mid-latitude westerlies provide the primary source of moisture to the Shigar region. Glaciers in the Ladakh region are small (1–10 km^2) cold-based subpolar glaciers, which are precipitation sensitive and sublimation dominated (Benn & Owen, 2002).

The arid/semiarid climatic setting of the Ladakh region is largely responsible for the preservation of very old landforms and sediment deposits (>400 ka; Hedrick et al., 2011; Orr et al., 2017, 2018; Owen et al., 2006) and slow rates of landscape change (<0.07 ± 0.01 mm/a; Dietsch et al., 2015; Dortch et al., 2011a). The investigated Gopal, Stok, and Amda catchments are three north-facing transverse catchments in the high-altitude desert landscapes of the northern Zanskar Range in Ladakh that retain small valley glaciers (Figures 2 and 3; Table 1). Karzok and Mentok are northeast-trending catchments that drain the Rupshu Massif in central Zanskar of the Ladakh region. Cirque glaciers occupy the upper reaches of these catchments.

The Lahul-Spiti and Kullu district catchments are located in Pir Panjal and Greater Himalaya ranges of the Himachal Pradesh in northern India. Precipitation is primarily sourced from the Indian summer monsoon (950–1,020 mm/a; Table 1). Glaciers are large, temperate and melt dominated, and fed by precipitation from the summer monsoon and mid-latitude westerlies (Benn & Owen, 2002; Su & Shi, 2002). The Urgos valley glacier extends throughout the upper reaches of a southeast trending tributary catchment of the Miyar basin in the Lahul-Spiti district (Figure 3). Panchi is a north-facing catchment with a small valley glacier, located north of the Keylong and Darcha villages. Shitidar and Batal are north facing tributary catchments with two glaciers each. The Chhota Shigri and Hamtah catchments are also north facing and are each occupied by one glacier. Beas Kund is a southeast trending catchment located on the southern slopes of the Pir Panjal Range in the Kullu district. Two valley glaciers are contained in this catchment. The Indian summer

monsoon also dominates annual precipitation in the Uttarkashi district of Uttarakhand, northern India, a region our study revisits and reanalyzes the rockwall erosion data of Orr et al. (2019).

2. Methodology

2.1. Topographic Analyses

Geomorphic maps of the 12 investigated catchments were prepared in the field and then refined using Advanced Spaceborne Thermal Emission and Reflection Radiometer (ASTER) global digital elevation models (GDEMs; 30-m-resolution), Landsat Enhanced Thematic Mapper Plus (ETM+) imagery and Google Earth imagery. Topographic parameters including catchment area, 3-km-radius relief, mean slope, hypsometry, and aspect were calculated using the Spatial Analyst Toolbox in ArcMap 10.1. These analyses were also conducted for Baltoro glacier system in the Shigar of Baltistan, Pakistan (Seong et al., 2009) and Bhagirathi glacier system in the Uttarkashi district of Uttarakhand, northern India (Orr et al., 2019) to enable comparisons between rockwall slope erosion and catchment parameters throughout the NW Himalaya.

2.2. Cosmogenic Nuclide Erosion Rate Theory for Rockwall Slopes

Production of cosmogenic ^{10}Be via neutron spallation occurs within the first few meters of the bedrock surface of the rockwall slopes and decreases approximately exponentially with depth. As material detaches from the rockwall slopes through erosion, new material moves into the zone of nuclide production (Balco et al., 2008; Lal, 1991; Uppala et al., 2005). The ^{10}Be inventory at the rockwall slope surface is the integrated cosmogenic nuclide production within quartz, during its exhumation through the zone of production Equation 1:

$$N\left(z\right) = \left(\frac{P_0}{\lambda + E\ /\ z_*}\right) e^{z/z^*} \tag{1}$$

N is the measured nuclide concentration at depth z, Po is the nuclide surface production rate, z^* is the e-folding length scale for the falloff of production with depth from the surface ($z_* = \Lambda/\rho$, where Λ is the spallogenic mean free path, and ρ is the target material density), E is the erosion rate, and λ is the radiogenic decay constant.

Rates of rockwall slope erosion can be inferred by measuring cosmogenic ^{10}Be concentrations within medial moraine sediment. In our study areas, medial moraines form within the glacier ablation zones as a result of englacial sediment melt out. This sediment is sourced and transferred from accumulation zone rockwall slopes to the glacier surface via rockfall processes and avalanching, before being transported englacially to the equilibrium line of the glacier and exhumed to the surface (Dunning et al., 2015; Goodsell et al., 2005; MacGregor et al., 2009; Matsuoka & Sakai, 1999; Mitchell & Montgomery, 2006; Figure 1). The ^{10}Be concentration of the medial moraine sediment reflects the averaged nuclide inventory of the source rockwall slopes. Due to the, stochastic nature of rockwall slope erosion, the ^{10}Be concentrations across the rockwalls are unlikely to be spatially uniform. The mean concentrations of these rockwall slopes are instead considered steady in time and linked to the mean erosion rate (Ward & Anderson, 2011).

$$E_{\mathrm{RS}} = \frac{P_0 z_*}{N} \tag{2}$$

The medial moraine nuclide concentrations and rockwall slope production rates are used to calculate the rockwall slope erosion rate (E_{RS}; Equation 2; Balco et al., 2008; Granger et al., 1996; Lal, 1991). The longer the original sampled material has remained within the production zone of the rockwall slopes before being transferred to the glacier surface, the greater the ^{10}Be concentration measured in the medial moraine sediment, and therefore the slower the inferred rockwall slope erosion rate. This approach to quantifying rockwall slope erosion accounts only for the spallogenic component of incoming cosmic rays and assumes a negligible loss of ^{10}Be due to radioactive decay, and steady-state erosion and ^{10}Be production over time (Von Blanckenburg, 2005). Further details of this methodology and its assumptions are provided by Supporting information S1 and in Ward and Anderson (2011) and Sarr et al. (2019).

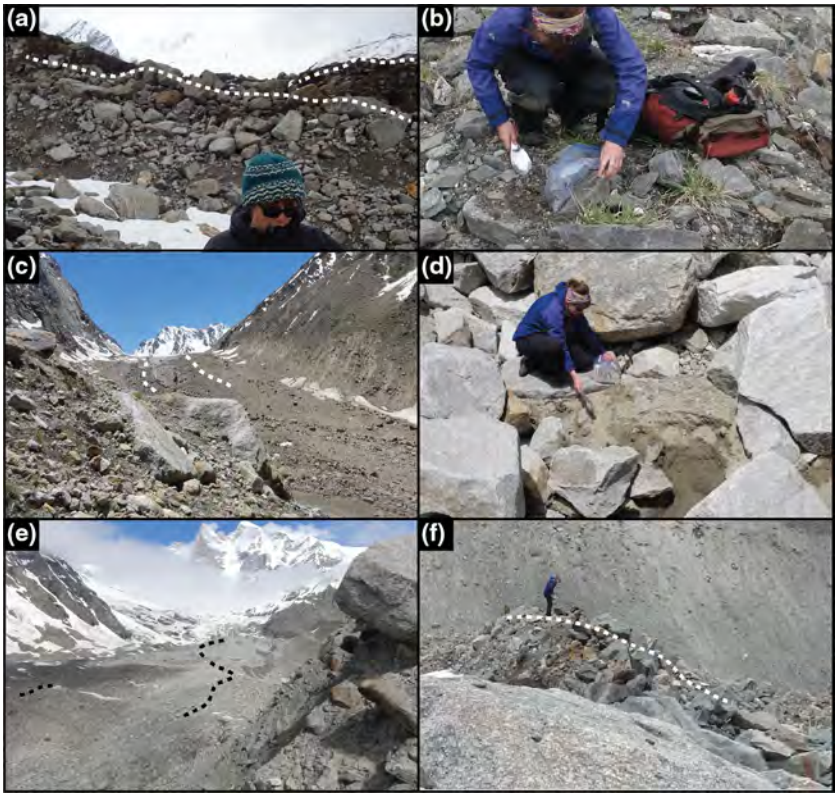

Figure 4. Views of medial moraines and sampling locations for three investigated catchments (white and black dashed lines outline medial moraine ridges). (a) Beas Kund medial moraine, (b) sampling of G_{Bea1} in Beas Kund, (c) Chhota Shigri medial moraine, (d) sampling of G_{Cht5} of Chhota Shigri, (e) Urgos medial moraine, (f) sampling of G_{Urg2}.

2.3. Cosmogenic Nuclide Analyses

Orr et al. (2019) argue that the rates of rockwall slope erosion in the upper Bhagirathi catchment in the Uttarkashi district of Uttarakhand are best represented by the rates derived from the centermost medial moraine of Gangotri glacier. This is because the ^{10}Be concentrations of the medial moraine fall within uncertainty of each other. Moreover, the concentrations from the other medial moraines are shown to be affected by input from lateral moraines and hillslopes along the ablation zone of the glacier. The study recommends that multiple samples should be taken from each medial moraine and/or glacier to constrain and evaluate any variability in rockwall slope erosion throughout the catchment headwaters. Two or fewer samples are only appropriate when the medial moraine is well preserved with steep relief ridges, has no interaction with ablation zone slopes and where other sampling locations do not fit these criteria. With these recommendations in mind, we carefully collected between one and five samples from stable and well-defined medial moraine ridges in each of the 12 catchments studied (Figures 3 and 4). Each sample location was ≥ 200 m^2 in area, to avoid sampling from a single source slope or rockfall event (see Supporting information S1). Approximately 3 kg of sediment with a grain size of <3 cm (clay-coarse gravels) was collected for each sample using bulk sediment sampling methods of Gale and Hoare (1991). Detrital samples of this grain size are shown to infer time-averaged erosion rates effectively, and for this study, are representative of the processes that contribute to rockwall slope denudation (Delunel et al., 2010; Lal, 1991; Puchol et al., 2014; Seong et al., 2009; Tofelde et al., 2018). Each sample was named using the initial term "*G*" for "glacier" followed by an abbreviated term for the catchment name. For glaciers with more than one sample, the samples were numbered in ascending order from the glacier snout. For example, the G_{Cht1} sample was located closest to the snout of Chhota Shigri in Lahul-Spiti, whereas G_{Cht5} was located farthest up-glacier.

Each sample was crushed and sieved in the Sedimentology Laboratories at the University of Cincinnati. A sample aliquot with equal mass input from each grain size fraction was created for each sample to avoid any one grain size from being overrepresented in the ^{10}Be analysis. The sample aliquot was crushed, sieved and

the 250–500 μm fraction was retained for processing. The extraction of quartz and ^{10}Be isolation and purification was conducted at the Geochronology Laboratories at the University of Cincinnati, using the chemical procedures of Nishiizumi et al. (1989), Von Blanckenburg et al. (2004), and Wittmann et al. (2016). The ^{10}Be/^{9}Be was measured using accelerator mass spectrometry at the Purdue Rare Isotope Measurement (PRIME) Laboratory at Purdue University (Sharma et al., 2000). Native ^{9}Be was measured via ICP–OES for each sample upon the recommendations of Portenga et al. (2015). The total ^{9}Be, including native ^{9}Be, rather than just the ^{9}Be carrier, was then used to calculate the ^{10}Be concentrations for the data set.

This method for quantifying erosion assumes that sediment storage at the rockwall slopes of each catchment is limited and that the transport of sediment from the rockwall to the medial moraine is rapid (Von Blanckenburg, 2005). Ward and Anderson (2011) developed an analytical expression to quantify the accumulation of cosmogenic nuclides during the transport of sediment from the source rockwall to the medial moraine. They found that ^{10}Be accumulation during the burial, englacial transport, and exhumation of sediment to the glacier surface was negligible in landscapes with denudation rates ≤1 mm/a. This model was implemented in our study because some of the records of erosion local to our investigated catchments, particularly in Uttarakhand, exceed this threshold (0.13–5.37 mm/a; Lupker et al., 2013; Scherler et al., 2014; Vance et al., 2003). Moreover, the glaciers of this study share similar glacier geometries, surface velocities and debris cover characteristics as to those described in the study by Ward and Anderson (2011). The modeled ^{10}Be accumulation during this transport was then subtracted from the total ^{10}Be sample concentration for each sample, before deriving the rockwall slope erosion rates (Supporting information S1; Table S1).

Rockwall slope erosion rates were calculated using Equations 1 and 2, which are described in detail by Balco et al. (2008), Dortch et al. (2011a), Granger et al. (1996) and Lal (1991). A 2σ uncertainty ascribed to the AMS results was propagated through the erosion rate calculations. Beryllium-10 production rates were calculated and corrected for topographic shielding for each rockwall slope using a combination of Delunel et al. (2010) and Dortch et al. (2011a) codes in MATLAB R2017.a, an ASTER 30-m GDEM (16-m vertical resolution), a calibrated sea-level high-latitude ^{10}Be spallogenic production rate from Martin et al. (2017; http://calibration.ice-d.org/) and a ^{10}Be half-life of 1.387 Ma (Chmeleff 2010; Korschinek 2010). Ward and Anderson (2011) and others have demonstrated that muonic production of ^{10}Be within amalgamated supraglacial debris sourced from the rockwall is negligible, and for the process timescales of rockwall slope erosion can be omitted from our calculation scheme (Akçar et al., 2014; Braucher et al., 2003; Sarr et al., 2019).

Widespread avalanching and minimal snow retention on the steep rockwall slopes within our study areas reduces our concern about the effects of snow shielding on the erosion data set. Scherler et al. (2014) estimated the impact of snow shielding on nuclide concentrations using remote sensing derived observations of snow cover duration and field-based measurements of annual daily snow depth in Uttarakhand, northern India. These data are unavailable for our entire study area. However, we have applied a 5.3% correction to our erosion rates; the mean correction value made by Scherler et al. (2014) for 10 catchments in Uttarakhand with similar topographic and climatic characteristics to our study area. This correction does not change any broad trends in the erosion data set (Table 4). However, due to the ambiguity attached to these correction estimates and the variability in mean annual precipitation across our study area, we prefer to use the uncorrected erosion rates herein.

2.4. Statistical Analysis of Erosion Data set

We calculated the Pearson Correlation Coefficient values (p) between the ^{10}Be rockwall slope erosion rates and climatic, topographic, tectonic and geologic parameters. A p value of <0.01 (at >99% confidence level) was applied. Each considered parameter has proven to influence rockwall and/or slope stability in other alpine regions (Krautblatter & Moore, 2014; McColl, 2012). In addition, we used Principle Component Analysis (PCA) to identify and evaluate the possible controls of rockwall slope erosion in the NW Himalaya (The R Core Team, 2018; Supporting informations S3 and S4). This approach has been successfully applied in other studies to identify and evaluate the nature and magnitude of the environmental and landscape response to changes in climate (Edwards & Richardson, 2004; Sagredo & Lowell, 2012; Seaby & Henderson, 2014). The topographic parameters included catchment and glacier area, mean slope of each catchment, rockwall and glacier, catchment 3-km-radius relief, mean catchment and snowline elevation, and glacier aspect. Climatic

variables included mean annual precipitation (weather stations [as referenced in Table 1] and TRMM [1998–2009]) and temperature (weather stations and CRU2.0 [as referenced in Table 1]), mean rockwall slope temperature and minimum catchment temperature. Catchment specific temperatures were calculated using an adiabatic lapse rate of 7°C/km and methods outlined in Orr et al. (2019). Additional variables, such as sample grain size and mean apatite fission track (AFT) cooling age (as referenced in Table 5), were also included within these analyses. The latter enables us to identify correlations between modern erosion rates and regional exhumation histories on the million-year timescale. The Uttarkashi data set (Kirti, Bhagirathi) was not included in these analyses because the rockwall slope erosion rates characterize an extensive basin system with numerous tributary catchments, rather than a single catchment as the remaining data set does. This data set is examined in more detail in the discussion section below. P-values were also calculated between rockwall slope erosion rates and catchment parameters for Ladakh and Lahul-Spiti as discrete regions (Supporting information S4). The other studied districts were not subject this regional analysis because the data sets are restricted to only one or two catchments.

3. Results

Catchment relief is subdued in the Ladakh region study areas in Jammu and Kashmir (0.7–1.0 km), despite the imposing, high-altitude mountain peaks, and rockwalls (>5,500 m asl) that mark the headwater limits of each catchment (Table 2). The mean rockwall slopes range between 26.3 ± 12.4 and 35.2 ± 15.5°. The topography of the Lahul-Spiti region in Himachal Pradesh is more severe than Ladakh, even with lower mean elevations (<4,500 m asl); the investigated catchments are larger (13.9–44.9 km^2), and have greater relief (1.2 ± 0.3–1.8 ± 0.5 km) and mean rockwall slopes (32.8 ± 12.8–47.2 ± 11.9°).

The ablation zones of the Lahul-Spiti and Kullu glaciers are partially to completely covered by debris, whereas in Ladakh, coverage is <30% of the glacier surfaces (Figure 4; Table 3). Beryllium-10 sample concentrations for the Ladakh and Lahul-Spiti/Kullu catchments range from $6.0 \pm 0.7 \times 10^4$ to $260.0 \pm 12.5 \times 10^4$ at/g SiO_2 and $0.5 \pm 0.04 \times 10^4$ to $30.6 \pm 1.0 \times 10^4$ at/g SiO_2, respectively (Figure 3; Table 4). On average, ~1% of the total ^{10}Be concentration of each sample was the result of ^{10}Be accumulation during transport from the source rockwall slopes to the medial moraine. For our study, this necessary correction to the final ^{10}Be concentrations had a negligible impact on the derived erosion rates (Table 4; Supporting information S1). Rates of rockwall slope erosion for the Ladakh region ranged between 0.02 ± 0.004 and 1.0 ± 0.2 mm/a, while rates in Lahul-Spiti/Kullu ranged from 0.2 ± 0.02 to 7.5 ± 1.0 mm/a (Figures 3 and 5; Table 4).

The catchment parameters with the most statistically significant relationship with rockwall slope erosion include mean rockwall slope, mean catchment and snowline elevation, mean annual precipitation, mean annual temperature, and mean AFT cooling age (Table 5). For the district-specific analysis, the same parameters are strongly correlated with rockwall slope erosion in Ladakh ($p = <0.01$; Supporting information S4). None of the parameters have a strong statistical correlation with the inferred erosion rates for the Lahul-Spiti district.

4. Discussion

ckwall erosion rates vary by up to two orders of magnitude throughout the NW Himalaya (0.02 ± 0.004–7.6 ± 1.0 mm/a; Figure 5). This is perhaps unsurprizing, considering the inherent complexities of periglacial-glacial environments, the application of cosmogenic nuclide analysis in these settings, and the range and variability in denudation recorded for this region (e.g., Scherler et al., 2014; Thiede & Ehlers, 2013; Vance et al., 2003). No relationship is apparent between ^{10}Be concentration and proximity of sample location to either a glacier margin or snout. Variability in ^{10}Be within the catchments is likely because the medial moraine sediment is poorly mixed and/or has a nonproportional sediment supply from the rockwall that is dominated by stochastic rockfall events (Muzikar, 2008; Small et al., 1997; Ward & Anderson, 2011).

The strong variability in physical settings of the catchments prevent any meaningful interpretations or comparisons between specific erosion rates. Moreover, time-averaged nuclide-derived erosion rates come with large uncertainties when characterizing local areas ($\leq 10^1$ km^2), which has been shown to underestimate the true rates (Sadler & Jerolmack, 2014; Willenbring et al., 2013; Yanites et al., 2009). Instead, we focus on the

Table 2
Catchment and Glacier Characteristics of the Investigated Catchments (Uncertainties Are Expressed to 2σ)

	Catchment characteristics							Glacier characteristics			
Catchment	Area (~km^2)	Max. elevation (m asl)	Relative relief[a] (km)	Mean slope[b] (°)	HI index[c]	Rockwall area (~km^2)	Mean rockwall slope (°)	Glacier area (~km^2)	Glacier aspect (°)	Mean slope[b] (°)	Modern ELA/ SE[d](m asl)
Gopal	4.9	5,920	1.0 ± 0.1	27.3 ± 12.6	0.4	4.2	33.9 ± 11.8	0.7	22.5	13.4 ± 6.9	5,420 ± 10
Stok	4.1	5,930	0.7 ± 0.1	26.6 ± 12.4	0.5	3.1	30.8 ± 11.8	1.0	45.0	14.4 ± 6.7	5,440 ± 10
Amda	7.0	6,000	0.8 ± 0.2	26.9 ± 15.7	0.5	5.3	35.2 ± 15.5	1.7	90.0	12.4 ± 6.6	5,525 ± 15
Karzok	3.9	5,970	0.9 ± 0.1	25.9 ± 12.2	0.5	3.6	26.3 ± 12.4	0.3	360.0	18.8 ± 10.9	5,550 ± 10
Mentok	10.3	6,200	0.9 ± 0.2	21.1 ± 13.6	0.4	7.6	35.5 ± 13.0	2.7	22.5	13.8 ± 7.8	5,610 ± 40
Urgos	30.3	6,290	1.2 ± 0.2	28.3 ± 13.9	0.4	26.6	32.8 ± 12.8	3.7	90.0	13.4 ± 8.5	4,830 ± 25
Panchi	20.5	5,945	1.3 ± 0.3	29.5 ± 14.0	0.4	16.0	34.8 ± 12.1	4.5	360.0	14.7 ± 8.7	4,560 ± 15
Shitidhar	22.2	5,945	1.8 ± 0.5	39.1 ± 14.5	0.4	20.7	42.8 ± 12.7	1.5	22.5	18.7 ± 7.3	4,050 ± 10
Batal	13.9	5,770	1.4 ± 0.2	34.3 ± 14.6	0.4	11.4	39.5 ± 12.2	2.5	22.5	15.2 ± 7.8	4,700 ± 15
Chhota Shigri	44.9	5,600	1.3 ± 0.3	29.4 ± 15.8	0.5	31.6	36.5 ± 14.8	13.3	360.0	16.2 ± 9.2	4,905 ± 25
Hamtah	33.1	6,155	1.2 ± 0.3	32.2 ± 14.9	0.4	28.3	39.2 ± 12.2	4.8	360.0	10.6 ± 6.0	4,450 ± 20
Beas Kund	17.6	5,140	1.6 ± 0.3	35.3 ± 16.3	0.4	16.6	47.2 ± 11.9	1.0	360.0	13.1 ± 8.7	3,725 ± 20

[a]3-km-radius relative relief. [b]Slope calculated from 0.001 km^2 catchment grid cells. [c]Strahler (1952) Hypsometric Index (mean elevation-min elevation/relief). [d]Mean of equilibrium-line altitudes (ELA)/snowline elevation (SE) calculated using Area-altitude (AA), Area-accumulation ratio (AAR: 0.4,0.5,0.6), and Toe-headwall ratio (THAR: 0.4,0.5) methods from Benn et al. (2005) and Osmaston (2005).

broad trends of this rockwall slope erosion data set for the NW Himalaya. Rockwall slope erosion decreases with distance north from the MCT; up to two orders of magnitude difference in erosion exist between Uttarakhand, Himachal Pradesh, Jammu and Kashmir, and Baltistan (Figure 5). The Urgos catchment in northern Lahul-Spiti slightly deviates from this trend with erosion rates of 3.2 ± 0.5 and 7.6 ± 1.0 mm/a, which are equivalent to those records in Kullu and southern Lahul-Spiti. The elevated rates may be attributed to increased annual precipitation in Miyar, which exceeds much of Lahul-Spiti (snowfall: 120–400 cm/a; Patel et al., 2018) and allows for more rapid erosion. Alternatively, the low ^{10}Be concentrations could be due to the input of fresh debris from the large, steep relief lateral moraines along Urgos glacier (Figure 4e and 4f).

The applicable timescales of this time-averaged data set, although varied (~0.1–24.6 ka), means that the erosion rates encompass recognized shifts in climate, sediment flux, glacier mass balance, and seismicity, which themselves operate across of timescales 10^{1-6} years (Barnard et al., 2004; Finkel et al., 2003; Owen and Dortch, 2014; Scherler et al., 2015). Between ~0.02 and ~8 m of lateral rockwall slope erosion is possible for a single millennium in the NW Himalaya. When these rates are extrapolated for the whole Quaternary period, an estimated ~2 km of rockwall retreat is accomplished in the NW Himalaya, which are similar estimates to the Sierra Nevada in the Western USA (Brocklehurst & Whipple, 2002). The magnitude of rockwall slope erosion evident in the NW Himalaya not only demonstrates the importance of slope erosion through periglacial processes, specifically frost cracking in high-altitude alpine settings, but also the significance that localized erosion has for understanding wider landscape change (Hales & Roering, 2005, 2007; Moore et al., 2009; Sanders et al., 2012, 2013; Small & Anderson 1998). The rates of rockwall slope erosion reflect, in part, the pace of topographic change at the catchment headwaters.

The magnitude of erosion, particularly in the GHS-S, is sufficient to affect the strength of hillslope-glacier coupling, catchment sediment flux and contribute to topographic change such as the production of relief, the migration of catchment divides, and the reconfiguration of drainage basins (Heimsath & McGlynn, 2008; MacGregor et al., 2009 *ibid;* Naylor & Gabet, 2007; Oskin & Burbank, 2005). The rockwall slope erosion rates share a significant association with mean rockwall slope: the greater the mean rockwall slope, the more rapid the erosion (Figure 6a, Table 5). This points to important feedbacks between these variables, where the rockwall slope angle and erosion rate limit one another. A tentative relationship can also

Table 3
Medial Moraine Morphology and Sediment Descriptions

	D.C[a]	Medial moraine description	Supraglacial diamict description
Gopal	R	Subdued moraine ridge; heterogeneous debris thickness (<5 mm−2 m)	Sandy-bouldery gravels with silt matrix; angular-subangular clasts of leucogranite and granitic gneiss
Stok	R	Subdued moraine ridge; heterogeneous debris thickness (<5 mm−2 m)	Bouldery gravels; angular-subangular clasts of leucogranite, granitic gneiss and schist
Amda	R	Moraine deposits along northern flank of Amda Kangri; heterogeneous debris thickness (<30 cm); some xerophytic shrubs	Sandy gravels with silt matrix containing interstitial ice; angular-subangular clasts of leucogranite and schist
Karzok	R	Subdued moraine ridge (<10 m wide); heterogeneous debris thickness (<5 mm−10 m)	Bouldery gravels with sandy matrix; very angular-subangular clasts of leucogranite, gneiss and schist.
Mentok	R	Moraine deposits at Mentok Kangri snout; heterogeneous debris thickness (<5 mm−3 m)	Bouldery gravels with sandy matrix; very angular-subangular clasts of leucogranite, gneiss and schist
Urgos	C	Distinct, steep relief medial moraine ridges; depressions and ice collapse features; heterogeneous debris thickness (<5 mm−5 m); tundra vegetation and large boulders (>2–0.25 m) along and slightly offset from ridges	Sandy-bouldery gravels with silt matrix containing interstitial ice; angular-subangular clasts of leucogranite and granitic gneiss
Panchi	C	Steep relief medial moraine ridge; surface depressions; large ice cliff at glacier snout	Sandy gravels with a silty-sand matrix; angular-subrounded clasts of schist
Shitidhar	P	Subdued moraine deposits; heterogeneous debris thickness (<5 mm−2 m)	Gravelly boulders with sandy matrix; very angular-angular clasts of leucogranite, gneiss and schist
Batal	C	Steep relief medial moraine ridge; ice cliffs; heterogeneous debris thickness (<5 mm−2 m)	Sandy-bouldery gravels with silt matrix, angular-subangular schistose clasts
Chhota Shigri	C	Distinct moraine ridges along length of ablation zone; heterogeneous debris thickness (<1 cm−1 m); large boulders (>5 m) located along moraine ridge; tundra vegetation	Bouldery gravels with sandy-silt matrix, angular-subrounded clasts of granite, granitic gneiss and schist
Hamtah	C	Distinct moraine ridges along length of ablation zone; heterogeneous debris thickness (<5 mm−>5 m); tundra vegetation	Bouldery gravels with sandy-silt matrix, angular-subrounded clasts of granitic gneiss and schis
Beas Kund	P	Steep relief medial moraine ridge, heterogeneous debris thickness (<5 mm−2 m).	Sandy-bouldery gravels; angular-subangular clasts of granite and gneiss

[a]Debris cover: C, Complete debris coverage of the glacier ablation zone; P, Partial coverage (>30% of ablation zone surface); R, Restricted coverage (<30% of ablation zone surface).

be recognized between relief and rockwall slope erosion; where catchments with the high-altitude peaks (>5,800 m asl), narrow ridgelines and high relief (>1.2 ± 0.2 km), record the highest rates of erosion. Part of this is because catchments with rockwall slope erosion rates >1 mm/a have mean rockwall slopes that exceed the 35° threshold, above which slopes are unable to retain regolith, snow or ice (Gruber & Haeberli, 2007; Nagai et al., 2013). This means that rockfall and avalanching is pervasive. More extensive glacier debris cover in these catchments compared to those with slower erosion demonstrate that coupling between rockwall and glacier is enhanced in catchments with steep accumulation areas, and that slope is important in moderating hillslope debris flux (Regmi & Watanabe, 2009; Scherler et al., 2011, Table 3). Other studies also recognize the importance of slope in landscape change, some of which argue that slope gradients

Journal of Geophysical Research: Earth Surface

10.1029/2020JF005619

Table 4

Medial Moraine Sample Details, ^{10}Be Concentrations and Inferred Rockwall Slope Erosion Rates for the Investigated Catchments

		Location[a]			Cosmogenic ^{10}Be data					Rockwall slope erosion rates			
Sample	Catchment	Latitude (°N)	Longitude (°E)	Elevation (m asl)	Quartz mass (g)	^{9}Be carrier mass, conc. (g, mg/g)	Native ^{9}Be (μg)	AMS ^{10}Be/^{9}Be ratio[b] (10^{-15})	^{10}Be concentration[c] (104 at/g SiO_2)	^{10}Be production rate (at/g SiO_2/ a)	Erosion rate (mm/a)	Snow corrected erosion rate[4] (mm/a)	Applicable time range (ka)
GGop1	Gopal	33.9865	77.4570	5,294	23.3326	0.3496, 1.0082	0	208.2 ± 7.0	20.9 ± 0.7	105.3 ± 13.6	0.3 ± 0.04	0.3 ± 0.04	2.0
GStk1	Stok	33.9668	77.4684	5,339	6.4552	0.3496, 1.0082	0	17.1 ± 2.3	6.0 ± 0.7	108.5 ± 14.0	1.1 ± 0.2	1.0 ± 0.2	0.6
GAmd1	Amda	33.6833	77.5910	5,340	25.8515	0.3490, 1.0255	0	120.0 ± 5.2	10.8 ± 0.3	107.1 ± 13.9	0.5 ± 0.1	0.6 ± 0.1	1.2
GAmd2	Amda	33.6837	77.5909	5,410	30.8093	0.3507, 1.0038	0	126.8 ± 4.2	9.5 ± 0.3	107.1 ± 13.9	0.7 ± 0.1	0.7 ± 0.1	0.9
GKar1	Karzok	32.9668	78.1775	5,362	22.6878	0.3492, 1.0255	0	2022.4 ± 34.3	213.0 ± 3.5	105.9 ± 13.7	0.03 ± 0.004	0.03 ± 0.004	20.1
GKar2	Karzok	32.9665	78.1776	5,367	13.2533	0.3506, 1.0038	0	1,205.0 ± 18.8	214.0 ± 3.2	105.9 ± 13.7	0.03 ± 0.004	0.03 ± 0.004	20.2
GKar3	Karzok	32.9663	78.1776	5,371	27.3612	0.3507. 1.0038	0.01	3,027.6 ± 146.2	260.0 ± 12.5	105.9 ± 13.7	0.02 ± 0.004	0.02 ± 0.004	24.6
GMen1	Mentok	32.9332	78.2107	5,506	29.3919	0.3497, 1.0255	0	406.4 ± 16.3	32.9 ± 1.2	107.5 ± 13.9	0.2 ± 0.03	0.2 ± 0.03	3.2
GUrg1	Urgos	32.8990	76.7646	4,420	17.6703	0.3505, 1.0038	0.01	16.3 ± 2.4	1.7 ± 0.2	90.2 ± 11.7	3.2 ± 0.5	3.0 ± 0.5	0.2
GUrg2	Urgos	32.8999	76.7635	4,434	20.0819	0.3491, 1.0038	0.01	9.5 ± 1.0	0.7 ± 0.02	90.2 ± 11.7	7.6 ± 1.0	7.5 ± 1.0	0.1
GPan1	Panchi	32.7244	77.3020	4,349	0.3987	0.3508, 1.0082	0	3.7 ± 1.2	19.3 ± 4.5	77.9 ± 10.1	0.2 ± 0.1	0.2 ± 0.1	2.5
GSht1	Shitidhar	32.4159	77.1049	3,568	4.6600	0.3494, 1.0082	0	6.8 ± 1.2	3.2 ± 0.4	60.2 ± 7.8	1.1 ± 0.2	1.1 ± 0.2	0.5
GBat1	Batal	32.3628	77.6012	4,310	11.3517	0.3505, 1.0082	0	147.4 ± 5.3	30.6 ± 1.0	81.0 ± 10.5	0.2 ± 0.02	0.2 ± 0.02	3.8
GBat2	Batal	32.3609	77.5981	4,368	6.3124	0.3495, 1.0082	0	9.8 ± 1.3	3.5 ± 0.3	81.0 ± 10.5	1.4 ± 0.2	1.3 ± 0.2	0.4
GCht1	Chhota Shigri	32.2639	77.5283	4,273	27.0872	0.3488, 1.0255	7.9	39.9 ± 5.3	3.2 ± 0.3	82.6 ± 10.7	1.5 ± 0.3	1.5 ± 0.3	0.4
GCht2	Chhota Shigri	32.2635	77.5283	4,281	26.4000	0.3496, 1.0038	4.7	46.1 ± 4.5	3.9 ± 0.3	82.6 ± 10.7	1.3 ± 0.2	1.3 ± 0.2	0.5
GCht3	Chhota Shigri	32.2629	77.5285	4,292	27.4440	0.3501, 1.0822	0	49.0 ± 16.5	4.2 ± 1.3	82.6 ± 10.7	1.2 ± 0.4	1.1 ± 0.4	0.5
GCht4	Chhota Shigri	32.2621	77.5287	4,316	18.7804	0.3487, 1.0255	40.5	12.0 ± 1.5	1.1 ± 0.004	82.6 ± 10.7	4.4 ± 0.6	4.2 ± 0.6	0.1
GCht5	Chhota Shigri	32.2611	77.5282	4,336	29.3671	0.3509, 1.0038	0	14.0 ± 1.3	1.0 ± 0.05	82.6 ± 10.7	5.1 ± 0.7	4.8 ± 0.7	0.1
GHam1	Hamtah	32.2643	77.3583	4,085	27.9648	0.3493, 1.0255	0.01	17.9 ± 1.5	1.3 ± 0.01	72.0 ± 9.3	3.4 ± 0.4	3.2 ± 0.4	0.2
GHam2	Hamtah	32.2640	77.3579	4,083	26.2989	0.3492, 1.0038	0	24.5 ± 3.2	2.0 ± 0.2	72.0 ± 9.3	2.1 ± 0.4	2 ± 0.4	0.3
GHam3	Hamtah	32.2635	77.3585	4,091	25.0875	0.3511, 1.0255	0.05	15.5 ± 3.4	1.2 ± 0.2	72.0 ± 9.3	3.7 ± 0.7	3.5 ± 0.7	0.2
GHam4	Hamtah	32.2626	77.3582	4,095	29.8146	0.3492, 1.0038	0	11.8 ± 2.2	0.8 ± 0.1	72.0 ± 9.3	5.5 ± 1.1	5.2 ± 1.1	0.1

Table 4
Continued

Sample	Catchment	Location[a] Latitude (°N)	Location[a] Longitude (°E)	Location[a] Elevation (m asl)	Cosmogenic ^{10}Be data Quartz mass (g)	^{9}Be carrier mass, conc. (g, mg/g)	Native ^{9}Be (μg)	AMS ^{10}Be/^{9}Be ratio[b] (10^{-15})	^{10}Be concentration[c] (104 at/g SiO_2)	Rockwall slope erosion rates ^{10}Be production rate (at/g SiO_2/ a)	Erosion rate (mm/a)	Snow corrected erosion rate[4] (mm/a)	Applicable time range (ka)
GBea1	Beas Kund	32.3543	77.0858	3,604	26.9295	0.3496, 1.0038	0.005	6.8 ± 0.9	0.6 ± 0.05	52.6 ± 6.8	5.7 ± 0.9	5.4 ± 0.9	0.1
GBea2	Beas Kund	32.3536	77.0863	3,594	25.8173	0.3499, 1.0038	0.015	9.2 ± 1.5	0.8 ± 0.1	52.6 ± 6.8	4.0 ± 0.7	3.8 ± 0.7	0.2
GBea3	Beas Kund	32.3534	77.0864	3,579	24.7578	0.3510, 1.0038	0.01	5.3 ± 0.8	0.5 ± 0.04	52.6 ± 6.8	6.8 ± 1.0	6.5 ± 1.0	0.1

[a]Location point is at the center of the ≥ 200 m^2 sampling area of each sample. [b]^{10}Be/^{9}Be ratios are corrected for background ^{10}Be detected in full procedural blanks (*GAmd1*, *GKar1*, *GMen1*; *GCht2,4*, *GHam1*, *GKar1*, *GMen1*: 3.14 ± 1.43 × 10^{-15}; *GCht3*: 3.14 ± 2.47 × 10^{-15}; *GAmd2*, *GKar2*, *GCht2,5*, *GHam2,4*: 1.55 ± 0.64 × 10^{-15}; *GBea1−3*: 4.15 ± 0.39 × 10^{-15}; *GKar3*, *GUrg1,2*: 3.41 ± 1.08 × 10^{-15}; *GGop1*, *GStk1*, *GPan1*, *GSht1*, *GBat1,2*: 4.15 ± 3.9 × 10^{-16}. [c]Accumulation of ^{10}Be during burial, englacial transport, and exhumation is calculated using methods detailed in Ward and Anderson (2011; see Supporting information S1). Accumulation is subtracted from the total concentration (^{10}Be [10^{4} at/g SiO_2]): Gopal- 0.0325; Stok- 0.0275; Amda- 0.0290; Karzok- 0.0250; Mentok- 0.0310; Urgos- 0.0225; Panchi- 0.0215; Shitidhar-0.0 130; Batal- 0.0205; Chhota Shigri- 220; Hamtah- 220; Beas Kund- 165 (see Supporting information S1).

can be used to infer rates of background denudation (Burbank et al., 2003; Finlayson et al., 2002; Ouimet et al., 2009; Portenga & Bierman, 2001; Scherler et al., 2011, 2014).

Rates of rockwall slope erosion in Uttarkashi and Ladakh districts are either equivalent to, or exceed by up to one order of magnitude, the local catchment-wide erosion and exhumation rates (Figure 6). Quaternary exhumation rates range between ~0.1 and 3 mm/a in the study areas (Thiede & Ehlers, 2013; Thiede et al., 2004). Catchment-wide rates for the Lahul-Spiti and Kullu districts are unavailable because much of the region remains glaciated (Owen & Dortch, 2014). Orr et al. (2019) caution that comparing these erosion datasets can be problematic as they refer to landscape change through a variety of erosional processes and across various spatial and temporal scales. Nevertheless, the order of magnitude difference in these rates shows that erosion at catchment headwaters in the NW Himalaya largely outpace the entire drainage basins (Naylor & Gabet, 2007; Oskin & Burbank, 2005), and that erosion can vary significantly across short distances downstream (Scherler et al., 2014). Time-averaged rates for small areas such as catchment headwaters and rockwall slopes are sensitive to short-term local change, including single mass wasting events, and are therefore expected to record more rapid rates of erosion than a catchment-wide perspective (Yanites et al., 2009; Willenbring et al., 2013). The Karzok catchment in central Zanskar of Ladakh deviates from this trend as the rockwall slope erosion either equals or is slower than the catchment-wide erosion and exhumation rates (Figure 6). The preservation and gradual reworking of landforms and sediment deposits that date to > 400 ka is likely affected by the low background denudation recorded in this region (Hedrick et al., 2011). A possible explanation is that sediment residence times exert a stronger control on the catchment-wide erosion signal in these ancient landscapes than the scale and various surface processes operating in the catchment area.

4.1. Controls of Slope Erosion

Considerable efforts have been made in recent years to define the parameters that control hillslope stability, and therefore determine the frequency and magnitude of mass wasting events (Ballantyne, 2002; Fischer et al., 2006, 2012; Hales & Roering, 2005; Matsuoka, 2001; Regmi & Watanabe, 2009; Sanders et al., 2012, 2013). The interactions between topography, climate, hydrology, geologic setting, and cryosphere dynamics have been shown to control rockfall activity. Of the catchment parameters that can be defined in the NW Himalaya, mean rockwall slope as already discussed, mean catchment and snowline elevation, mean annual precipitation, mean annual temperature, and mean AFT cooling ages show the strongest correlation with rockwall slope erosion rates (Figures 6 and 8; Table 5).

Catchments with the most rapid rockwall erosion have a greater proportion of the rockwall slope above the snowline than below, and larger glacier accumulation areas, than those with lower erosion rates. Aided by high gradient slopes that are set in part by erosion, field assessments, and satellite imagery suggest that snow and ice entrained debris is either removed from the rapidly eroding rockwalls via avalanching or is largely absent. Evidence of avalanching underlines the importance of snow processes and cover, whether set by climatic conditions or surface uplift, in the transfer of debris from the rockwall to the glacier system (Scherler et al., 2011, 2014).

Estimated surface temperatures of the rockwalls are similar to those considered optimal for mechanical weathering processes (−8 to −3°C), for example, freeze-thaw, frost cracking, and frost wedging (Brozović et al., 1997; Hales & Roering, 2005; Hewitt, 2002; MacGregor et al., 2009; Matsuoka, 2001; Matsuoka & Sakai, 1999, Table 1). The medial moraine sediment characteristics are consistent with sediment from the supraglacial realm, which have detached from source slopes by periglacial weathering processes

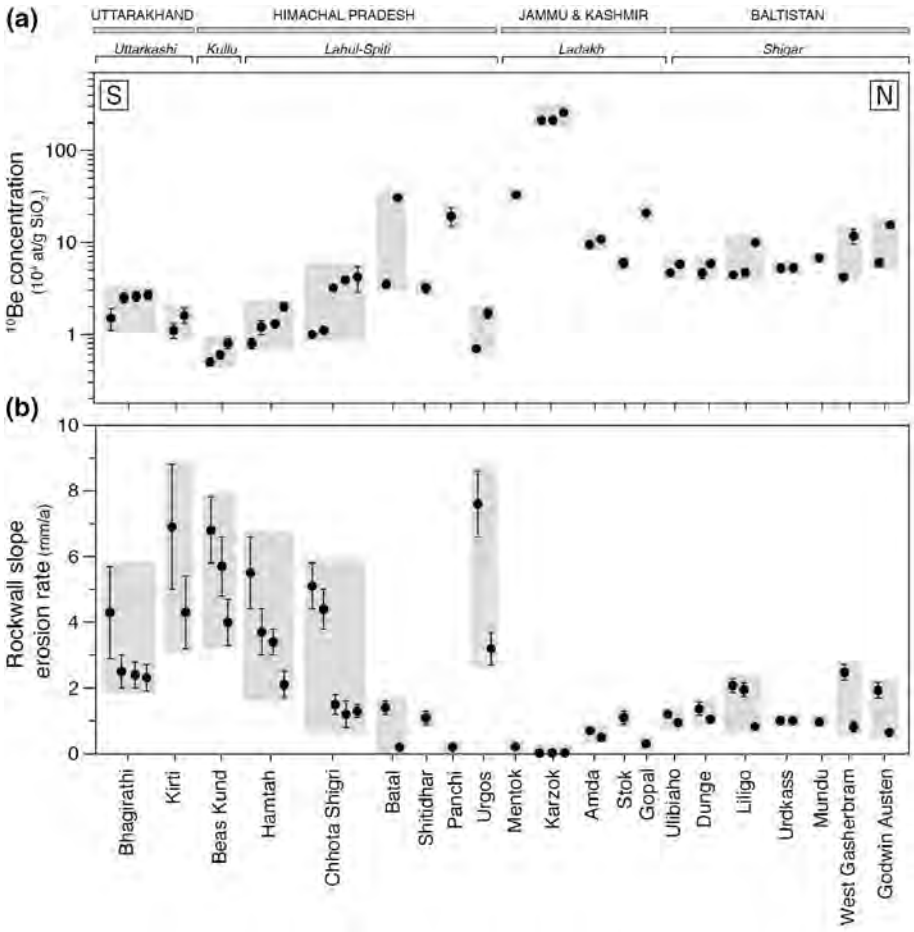

Figure 5. Sample ^{10}Be concentrations (a) and rockwall slope erosion rates (b) for the northwestern (NW) Himalaya. Uttarkashi (Bhagirathi glacier system) and Shigar (Baltoro glacier system) data sets are from Orr et al. (2019) and Seong et al. (2009), respectively. The black circles in this plot are data points – they are the concentration and erosion data points.

(Benn & Lehmkuhl, 2000; Benn & Owen, 2002; Hambrey et al., 2008; Lukas et al., 2012; Orr et al., 2019; Schroder et al., 2000, Table 3; Supporting information S5). Rates of periglacial erosion are likely further enhanced by seasonal and/or diurnal thermal variability in exposed bedrock surfaces of our investigated catchments, which is determined in part by the topographic steepness (Fischer et al., 2012; Gruber & Haeberli, 2007; Haeberli et al., 2017; Nagai et al., 2013). However, for high elevation catchments (>4,000 m asl) and/or rockwall slopes of our study area that lack an insulating layer of snow due to threshold slopes, bedrock surfaces can reach temperatures below −8°C, which inhibit further mass wasting (Ward & Anderson, 2011). This is tentatively reflected in the relationship between temperature and rockwall slope erosion; the catchments with lower regional temperatures record slower erosion rates (Figure 6c). The rockwall debris flux of each catchment is therefore likely influenced by the feedbacks between elevation, temperature, and slope.

A strong positive relationship between ^{10}Be-derived rockwall slope erosion and mean annual precipitation supports the view that the distribution and magnitude of Himalayan erosion and denudation is partly a function of orographically focused monsoon rainfall (Bookhagen & Burbank, 2006; Bookhagen et al., 2005a; Dey et al., 2016; Gabet et al., 2006; Theide et al., 2004; Wulf et al., 2010, Figures 6c and 7). The argument that precipitation provides a first-order control on the frequency and magnitude of mass wasting events in alpine settings is common (Dortch et al., 2009; Hovius et al., 2000; Iverson, 2000). Eppes and Keanini (2017) argue that the proficiency of mechanical weathering processes such as subcritical cracking is climate de-

Table 5
Pearson's Correlation Coefficient Values (p) Between ^{10}Be Rockwall Slope Erosion Rates and Catchment Parameters

		Rockwall slope erosion rate
	Max. Grain size (2)	0.7
Catchment charact.	Catchment area (>10)	0.0003
	Rockwall area (>10)	0.002
	Peak elevation (>10)	0.8
	Mean elevation (>10)	0.0001
	Snowline elevation (>10)	0.00006
	Catchment relief (>10)	0.2
	Catchment slope (>10)	0.006
	Rockwall slope (>10)	0.00002
Glacier charact.	Glacier area (>10)	0.02
	Glacier aspect (>10)	0.5
	Mean glacier slope (>10)	0.02
	Glacier velocity (5)	0.8
Climatic conditions	Mean annual precipe.(4)	0.0007
	Mean annual temp. (3)	0.000004
	Min. Catchment temp. (3)	0.5
	Mean rockwall temp. (>10)	0.1
	Lithology (2)	0.8
	Mean AFT age3 (8)	0.0000030

Notes. Catchment and glacier characteristics data set detailed in Table 2 and Supporting information S3. Climatic data set detailed in Table 1 and Supporting information S3. Mean of AFT ages from Jain et al. (2000), Kristein et al. (2006, 2009), Searle et al. (1999), Schlup et al. (2003, 2011), Sorkhabi et al. (1996), Thiede et al. (2004, 2005, 2006, 2009), Van Der Beek et al. (2009), Vannay et al. (2004), and Walia et al. (2008, Supporting information S3) AFT, apatite fission track.

pendent, and specifically limited by moisture. Sources of moisture in alpine environments include snowfall, rainfall, and melt water. Although rockwall slope erosion is certainly influenced by the availability of moisture and is sensitive to the microclimatic conditions of each catchment, its distribution throughout the NW Himalaya cannot be fully explained by precipitation. A five fold decline in precipitation occurs between the first topographic high of the Lesser Himalaya (900 ± 400 m asl) and the interior ranges of the orogen (Bookhagen et al., 2005a, 2005b; Bookhagen & Burbank, 2006, Figure 7). If precipitation were the primary control of rockwall slope erosion as we hypothesized, then we would expect to find that our maximum erosion rates coincide with maximum rainfall, and that a notable decline in these rates would be observed with distance north into the Greater Himalayan interior. However, our results show that this is not the case. Scherler et al. (2014) make a similar observation, where the highest catchment-wide rates in Uttarakhand are also located north of the precipitation maxima. To further, emphasize this point, there is an order of magnitude difference in the rockwall slope erosion rates between the GHS-N and the Tethyan Himalayan, yet a small decline in annual precipitation of < 300 mm.

Since the Late Miocene the steep orographic barrier of the Himalaya has restricted the northward advancement of moisture (Bookhagen et al., 2005a; Wulf et al., 2010), therefore preventing any subsequent major shift in the overall intensity or distribution of precipitation (Bookhagen & Burbank, 2010; Bookhagen et al., 2005a; Boos & Kuang, 2010; Thiede & Ehlers, 2013). The overall pattern in rockwall slope erosion throughout the NW Himalaya is therefore unlikely to be an artifact of a previous climatic regime, despite short-term fluctuations in monsoon strength during the Quaternary potentially affecting rockfall activity on the catchment scale (Demske et al., 2009; Fleitmann et al., 2003; Gupta et al., 2003; Thompson et al., 1997). One major concern in evaluating the role of climate in long-term landscape change is that the denudation records are averaged across million-year timescales and are therefore unable to account for the importance or variations in the Indian summer monsoon (Bookhagen et al., 2005a; Thiede & Ehlers, 2013). This study, is able to show that erosion records that reflect landscape change on timescales that would be sensitive to fluctuations in monsoon strength (10^{2-5} years), that is, rockwall slope and catchment-wide erosion, are not unilaterally controlled by precipitation.

The patterns in rockwall slope erosion rates are most closely associated with regional AFT cooling ages (Figures 6d and 7; Table 5). Much attention has been paid to understanding the patterns of cooling ages and exhumation rates in the Himalaya, and the feedbacks between tectonics and climate that are responsible for the distribution and intensity of Himalayan denudation across million-year timescales (Schelling & Arita, 1991; Srivastava & Mitra, 1994; Thiede & Ehlers, 2013). Many studies have argued that denudation is primarily governed by climate; orographic precipitation causes rapid erosion and exhumation along the Himalayan front and Lesser Himalaya (Biswas et al., 2007; Grujic et al., 2006; Kumar et al., 2018; Sharma et al., 2017; Thiede et al., 2004; Zeitler et al., 2001). However, young AFT ages (<10 Ma) and rapid rates of exhumation throughout the Lesser Himalaya and GHS-S instead reflect a close interaction between tectonics, denudation and monsoon-enhanced erosion, rather than just the latter (e.g., Thiede et al., 2004; Vannay et al., 2004; Wobus et al., 2003). Coupling between climate and tectonics becomes less evident farther into the Greater Himalayan interior; while the GHS-N becomes progressively more arid, the AFT ages remain <17 Ma and exhumation rates > 5 mm/a (Schlup et al., 2003; Thiede & Ehlers, 2013, Figure 7). The pattern in AFT ages and inferred exhumation histories for the NW Himalaya, like our rockwall slope erosion data set, cannot therefore be fully explained by precipitation. Instead, there is the argument that the patterns of Himalayan denudation are instead a function of tectonically controlled rock uplift; the result of crustal

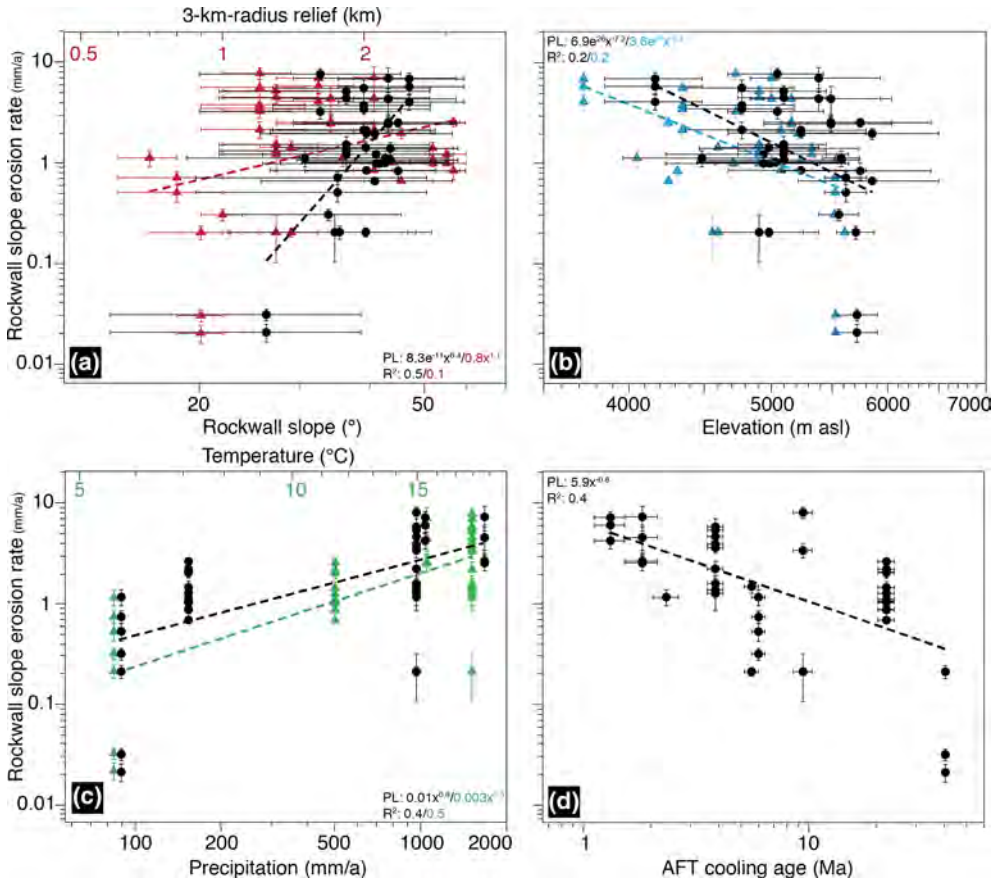

Figure 6. Rockwall slope erosion rates and catchment parameters. (a) Mean rockwall slope (black points) and 3-km-radius relief (red triangles). (b) Mean elevation (black points) and snowline elevation (blue triangles). (c) Mean annual precipitation (black points) and mean annual temperature (green triangles). (d) Mean AFT cooling ages (black points). AFT, apatite fission track; PL, Power Law function.

wedge deformation from the Indo-Eurasian collision and the flat-ramp-flat geometry of the Main Himalayan Thrust (e.g., Burbank et al., 2003; Bollinger et al., 2006; Godard et al., 2014; Herman et al., 2010; Robert et al., 2011). The lateral and vertical transport of rock over the ramp since the late Miocene has resulted in rapid and continuous exhumation, and the generation of steep topographic relief (Cattin & Avouac, 2000; Godard et al., 2004; Lavé & Avouac, 2000, 2001). Young AFT cooling ages and rapid rates of exhumation are therefore focused throughout the Lesser Himalaya and GHS-S (Figure 7). This is consistent with our patterns in rockwall slope erosion, therefore indicating that tectonically driven rock uplift throughout the NW Himalaya is likely to provide a major control on patterns of denudation since the late Paleogene, and also influence late Quaternary records of erosion (Scherler et al., 2011, 2014). The climatic parameters of precipitation and temperature are therefore likely secondary controls. Moreover, this confirms that similar casual relationships between rock uplift and erosion operate throughout the glaciated and non-glaciated regions of the NW Himalaya.

PCA indicate that ~68% of the variance observed in rockwall slope erosion rates in the NW Himalaya can be explained by the six parameters discussed above (mean rockwall slope, mean catchment and snowline elevation, mean annual precipitation, mean annual temperature, and mean AFT age; Figure 8). To explain the remaining variance, other parameters must be considered. Rockwall lithology, rock strength and mass quality, and jointing and structure, for example, affect the thresholds for mass wasting and have been shown to govern hillslope debris flux and rates of erosion (Anderson, 1998; Augustinus, 1995; Fischer et al., 2010; Hales & Roering, 2005; Hallet et al., 1991; MacGregor et al., 2009). Rockfall activity in the investigated catchments is therefore likely affected by the erodibility of the rockwall and the periglacial processes acting

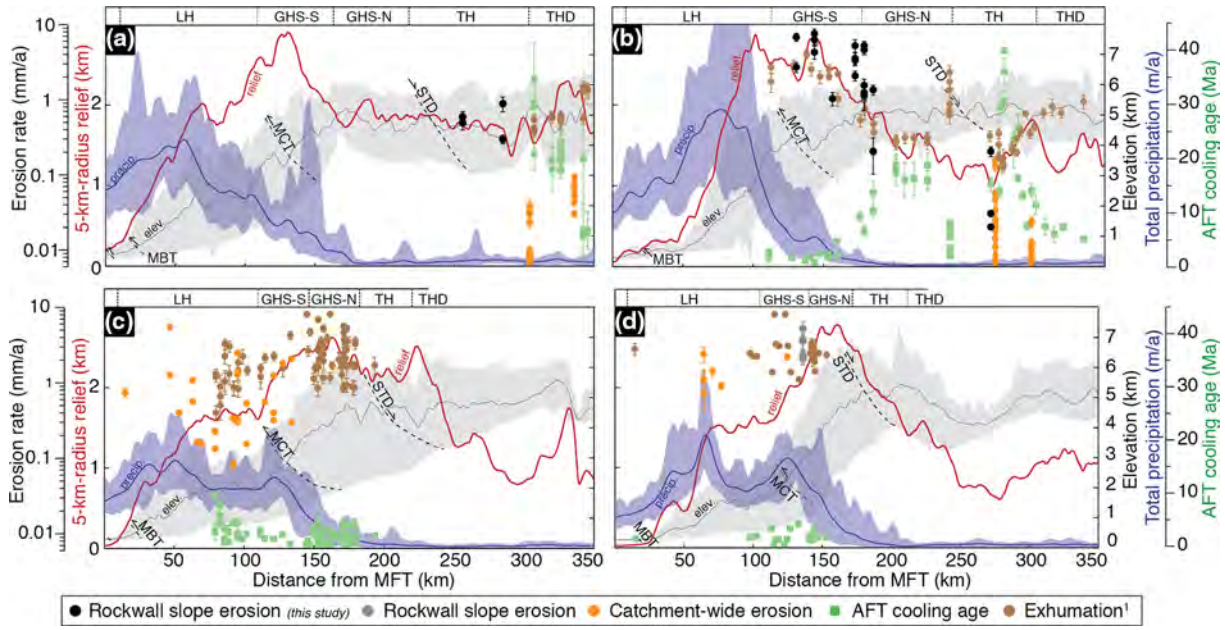

Figure 7. Erosion, relief and precipitation of the NW Himalaya with distance from the MFT (data sets from Bookhagen & Burbank, 2010). TRMM 2B31 precipitation data is plotted using the unit of m/a, and not mm/a as in text. Swath locations outlined in Figure 1a (GHS-S/N, Greater Himalayan sequence South/North; LH, Lesser Himalaya; TH, Tethyan Himalaya; THD, Tethyan Himalaya Dome). [1]: Exhumation rates (use erosion rate *y*-axis) are inferred from AFT cooling ages as referenced below, an AFT cooling temperature of 120°C, and a geothermal gradient of 25°C/km. (a) Swath 1 (S1). Rockwall slope erosion: this study; catchment-wide erosion: Dortch et al. (2011a), Dietsch et al. (2015); AFT cooling ages: Kristein et al. (2006, 2009). (b) Swath 2 (S2). Rockwall slope erosion: this study, Scherler and Egholm (2020); catchment-wide erosion: Dortch et al. (2011a), Dietsch et al. (2015), AFT cooling ages: Schlup et al. (2003, 2011), Thiede et al. (2006), Walia et al. (2008). (c) Swath 4 (S4). Catchment-wide erosion: Scherler et al. (2014); AFT cooling ages: Jain et al. (2000), Thiede et al. (2004, 2005, 2009), Vannay et al. (2004). (d) Swath 5 (S5). Rockwall slope erosion: Orr et al. (2019); catchment-wide erosion: Vance et al. (2003), Lupker et al. (2012); AFT cooling ages: Sorkhabi et al. (1996), Searle et al. (1999), Thiede et al. (2009). AFT, apatite fission track; MFT, Main Frontal Thrust.

upon it (Eppes & Keanini, 2017; Heimsath & McGlynn, 2008; Moon et al., 2017). The significance of this parameter in the patterns of rockwall slope erosion on the regional scale is however less clear. Previous work has argued that the difference in rock strength between the crystalline sequences of the Lesser and Greater Himalaya is negligible, and has little influence upon the denudation histories of the orogen (Burbank et al., 2003; Scherler et al., 2011, 2014).

Mass wasting events are closely associated with earthquakes and/or persistent microseismicity as documented by various studies throughout High Asia (e.g., Dortch et al., 2009; Hovius et al., 2000; Lupker et al., 2012; Menunier et al., 2008). For example, earthquakes in Uttarakhand such as the 1991 Uttarkashi (M 6.1; Bali et al., 2003; Valdiya, 1991) and 1999 Chamoli (M 6.6; Rajendran et al., 2000) events are found to trigger mass redistribution on a scale that affects short-term erosion rates (Bali et al., 2003; Scherler et al., 2014). The frequency of rockfall events and therefore rates of rockwall slope erosion in our catchments is therefore likely to be influenced in part by local tectonic activity.

A further candidate for rockwall slope erosion control is glaciation and glacial erosion; vertical incision and the debuttressing of slopes can lead to enhanced slope instability and failure (Fischer et al., 2010; Heimsath & McGlynn, 2008; MacGregor et al., 2009; Naylor & Gabet, 2007). Large, erosive temperate glaciers occupy catchments with rapid rates of rockwall slope erosion, while slower rates are from catchments with less erosive, subpolar glaciers (Owen & Dortch, 2014). Past retreat and expansion of glacier ice may also have contributed to the evolution of the rockwalls; the downwasting of ice may encourage the unloading of slope debris, while a greater glacier volume may see an increase in glacial erosion processes acting upon the slope (Fischer et al., 2006, 2010, 2012; Herman et al., 2010). For example, the Hamtah glacier in Lahul-Spiti has retreated ~90 m in the last ~200 years, during which time rockwall slope erosion rates have exceeded 3 mm/a (Tables 1 and 4; Figure 5; Saha et al., 2018). Rockwall slope erosion is therefore likely a critical component of the catchment headwater's response to shifts in glaciation, where the redistribution of stress from

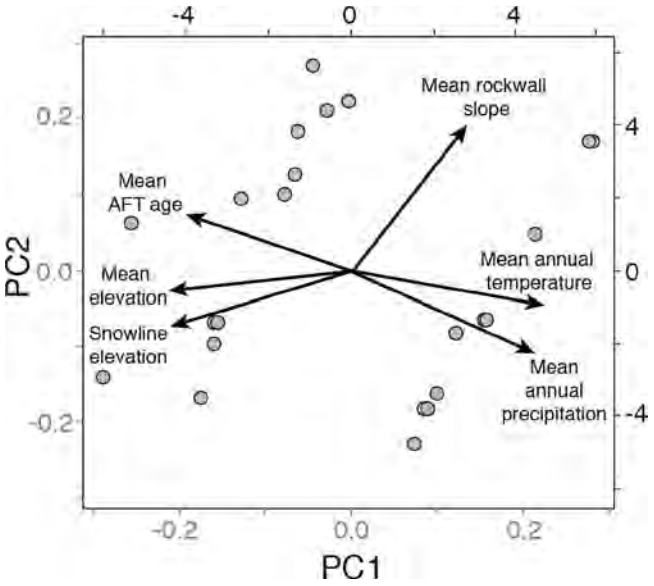

Figure 8. PC1/PC2 plot for the catchment parameters that contribute to the distribution and magnitude of the rockwall slope erosion. Parameters with strongest correlation with erosion are labeled. Proportion of variance: PC1 (0.68), PC2 (0.17), PC3 (0.07), and PC4 (0.04). These are the data points generated by the PCA analysis.

changing ice extents likely decreases slope stability (Gallach et al., 2018; McColl, 2012). These processes are part of a complex feedback; supraglacial debris cover above a critical thickness can act to insulate glacier ice, while a thinner layer can enhance melt by decreasing the albedo of the glacier surface (Ostrem, 1959). The erosion and delivery of debris from the rockwall slopes to the glacier can therefore affect surface melt rates, the mass balance of the glacier, and more broadly the glacier's sensitivity to environmental change (Anderson et al., 2011; Immerzeel et al., 2014; Gibson et al., 2017). To complete the feedback; glaciation and glacier dynamics regulate glacial erosion processes and local climatic conditions, which are both parameters that are shown to affect rockwall slope stability (Anderson et al., 2018; Heimsath & McGlynn, 2008; McColl, 2012).

Rather than a single control, we have confirmed the initial conclusions of Orr et al. (2019) by finding that rockwall slope erosion is instead more likely the result of longstanding feedbacks between climate, tectonics, topography, and surface processes which are specific to each catchment. The relative importance of these various parameters in driving rockwall slope erosion will likely vary across space and time. For example, the recognized relationship between rockwall erosion and slope for the NW Himalaya does not extend to the Lahul-Spiti district, if it were considered a discrete region. Only in Ladakh do the steepest catchment and rockwall slopes record the most rapid rates of erosion. This does not mean that rockwall erosion is unaffected by slope in Lahul-Spiti; however, it does suggest that other parameters are also necessary to explain the patterns of erosion. No parameters discussed show a strong correlation with rockwall slope erosion in Lahul-Spiti (Supporting information S4). Explanations for this might be that the erosion of rockwalls is influenced by a combination of parameters which together affect rockwall slope stability, or that this erosion is sensitive to undefined parameters such as glaciation and glacial processes (e.g., glacier type and dynamics, glacial erosion). Deciphering erosion controls may not be possible due to the inherent complexities of glaciated catchments in this district (e.g., rapid cycles of glacier retreat/advance, shifts in fluvial/meltwater discharge and erosion, variability in glacial/nonglacial sediment source-sink sedimentation; Adams et al., 2009; Bookhagen & Burbank, 2010; Bookhagen et al., 2006; Saha et al., 2018).

Controls of rockwall slope erosion may also be difficult to constrain across various temporal and spatial scales because for some catchments, once a threshold for a particular parameter has been met (e.g., moisture availability), rockwall slope erosion becomes predominantly limited by it. During a period of enhanced rainfall or monsoon along the Himalayan front for example (Bookhagen et al., 2005b; Clift et al., 2008), catchments with strongly contrasting geology and/or topography may display similar rockfall activity. In this case, the magnitude of precipitation is sufficient to govern rockwall slope stability and override any resistance to mass wasting (e.g., strong, nonerosive rock type or low gradient slopes). When averaged over time, these physically contrasting catchments will share a similar record of rockwall slope erosion. This may offer an explanation for why single high-magnitude events such as these, are viewed to be responsible for a significant proportion of the total landscape change in mountain environments (Craddock et al., 2007; Hasnain, 1996; Kirchner et al., 2001; Wulf et al., 2010). To tackle some of these outstanding questions, rockwall slope erosion controls should be evaluated for glaciated catchments with comprehensive geologic and climatic data and well constrained records of glacial history, topographic change, and mass wasting.

We suggest that, rockwall slope erosion is largely influenced by catchment-specific conditions that vary over temporal and spatial scales. However, our study is able to demonstrate that the broad spatial patterns in rockwall erosion follow long-term trends in denudation throughout the NW Himalaya, and is therefore broadly controlled by tectonically driven rock uplift. The climatic parameters of precipitation and temperature are therefore likely secondary controls. This suggests that, periglacial rockfall processes are part of the erosional response to structural change throughout the Himalayan-Tibetan orogen, and play a significant role within topographic change at catchment headwaters and the mass balance of the orogen. Overall, our

study further adds to the growing body of evidence in the wider Himalaya and other regions such as the northern Bolivian Andes that denudation patterns do not always follow gradients in precipitation (Burbank et al., 2003; Gasparini & Whipple, 2014; Godard et al., 2014; Scherler et al., 2014).

5. Conclusion

Rates of rockwall slope erosion are defined for 12 catchments in northern India, NW Himalaya and range between 0.02 ± 0.004 and 7.6 ± 1.0 mm/a. Rockwall slope erosion largely outpaces local catchment-wide erosion and exhumation, and is sufficient to affect catchment sediment flux, glacier dynamics, and topographic change, such as the production of relief, the migration of catchment divides, and the reconfiguration of drainage basins.

Erosion rates become progressively lower with distance north from the MCT; up to two orders of magnitude difference in erosion rates are observed between the Uttarkashi, Kullu, Lahul-Spiti, and Ladakh and Shigar regions. Rather than a single control, rockwall slope erosion on a catchment-by-catchment basis is largely influenced by longstanding feedbacks between climate, tectonics, topography, and surface processes. The relative roles of these parameters are likely to vary over various spatial and temporal scales.

Our study demonstrates that, like records of denudation in the NW Himalaya, the broad trend in rockwall slope erosion cannot be fully explained by the distribution of precipitation. Instead, rockwall slope erosion can be considered part of the erosional response to tectonically driven uplift, the product of Indo-Eurasian convergence, and structural geology. The distribution and magnitude of erosion applicable to geomorphic (10^{2-5} years) and geologic (10^{6} years) timescales in the NW Himalaya therefore suggests that tectonics, rather than climate, provide a first-order control on landscape evolution. Our study also demonstrates the importance of lateral rockwall slope erosion via periglacial processes in helping set the pace of topographic change at catchment headwaters of high altitude and high relief mountain ranges, and the significance that localized erosion has for understanding wider landscape change.

Data Availability Statement

All supporting data can be accessed through the GFZ Data Services at https://dataservices.gfz-potsdam.de/panmetaworks/review/26c9ad2dcd8617d7e18c8bb71b57b8e872a27eab88bcbf540b2d28db3d020d46/

Acknowledgments
E. N. Orr thanks the University of Cincinnati for providing tuition and stipend to support this work as part of E. N. Orr's doctoral thesis and the processing of samples for ^{10}Be dating. E. N. Orr would like to thank PRIME Laboratories at Purdue University for a seed grant for AMS measurements (NSF-EAR0919759). E. N. Orr also extends thanks to National Geographic, the Geological Society of America and the Graduate Student Governance Association, University of Cincinnati for research grants to conduct fieldwork. E. N. Orr and S. Saha thank T. Dorje and Discover Ladakh for providing logistical support in the field. L A. Owen thanks the University of Cincinnati for providing support for fieldwork. The authors would like to thank the Associate Editor Harrison Gray, Brent Goehring, and four anonymous reviewers for their detailed, constructive comments and suggestions, which greatly improved the manuscript.

References

Adams, B., Dietsch, C., Owen, L. A., Caffee, M. W., Spotila, J., & Haneberg, W. C. (2009). Exhumation and incision history of the Lahul Himalaya, northern India, based on (U–Th)/He thermochronometry and terrestrial cosmogenic nuclide methods. *Geomorphology*, *107*(3–4), 285–299. https://doi.org/10.1016/j.geomorph.2008.12.017

Akçar, N., Ivy-Ochs, S., Deline, P., Alfimov, V., Kubik, P. W., Christl, M., & Schlüchter, C. (2014). Minor inheritance inhibits the calibration of the ^{10}Be production rate from the AD 1717 Val Ferret rock avalanche, European Alps. *Journal of Quaternary Science*, *29*(4), 318–328. https://doi.org/10.1002/jqs.2706

Anderson, R. S. (1998). Near-surface thermal profiles in alpine bedrock: Implications for the frost weathering of rock. *Arctic and Alpine Research*, *30*(4), 362–372. https://doi.org/10.1080/00040851.1998.12002911

Anderson, R. S., Anderson, L. S., Armstrong, W. H., Rossi, M. W., & Crump, S. E. (2018). Glaciation of alpine valleys: The glacier-debris-covered glacier-rock glacier continuum. *Geomorphology*, *311*, 127–142. https://doi.org/10.1016/j.geomorph.2018.03.015

Anderson, L. S., Roe, G. H., & Anderson, R. S. (2014). The effects of interannual climate variability on the moraine record. *Geology*, *42*(1), 55–58. https://doi.org/10.1130/G34791.1

André, M. F. (2003). Do periglacial landscapes evolve under periglacial conditions? *Geomorphology*, *52*(1–2), 149–164. https://doi.org/10.1016/S0169-555X(02)00255-6

Augustinus, C. (1995). Glacial valley cross-profile development: The influence of in situ rock stress and rock mass strength, with examples from the Southern Alps, New Zealand. *Geomorphology*, *14*(2), 87–97. https://doi.org/10.1016/0169-555X(95)00050-X

Azam, M. F., Wagnon, Vincent, C., Ramanathan, A. L., Favier, V., Mandal, A., & Pottakkal, J. G. (2014). Processes governing the mass balance of Chhota Shigri Shigri Glacier (western Himalaya, India) assessed by point-scale surface energy balance measurements. *The Cryosphere*, *8*(6), 2195–2217. https://doi.org/10.5194/tc-8-2195-2014

Balco, G., Stone, J., Lifton, N., & Dunai, T. (2008). A complete and easily accessible means of calculating surface exposure ages or erosion rates from ^{10}Be and ^{26}Al measurements. *Quaternary Geochronology*, *3*, 174–195. https://doi.org/10.1016/j.quageo.2007.12.001

Bali, R., Awasthi, D. D., & Tiwari, N. K. (2003). Neotectonic control on the geomorphic evolution of the Gangotri Glacier Valley, Garhwal Himalaya. *Gondwana Research*, *6*(4), 829–838. https://doi.org/10.1016/S1342-937X(05)71028-5

Ballantyne, C. K. (2002). Paraglacial geomorphology. *Quaternary Science Reviews*, *21*(18–19), 1935–2017. https://doi.org/10.1016/S0277-3791(02)00005-7

Barnard, Owen, L., & Finkel, R. (2004). Style and timing of glacial and paraglacial sedimentation in a monsoon-influenced high Himalayan environment, the upper Bhagirathi Valley, Garhwal Himalaya. *Sedimentary Geology*, *165*, 199–221. https://doi.org/10.1016/j.sedgeo.2003.11.009

Barr, I. D., & Lovell, H. (2014). A review of topographic controls on moraine distribution. *Geomorphology*, *226*, 44–64. https://doi.org/10.1016/j.geomorph.2014.07.030

Bashir, F., & Rasul, G. (2010). Estimation of water discharge from Gilgit Basin using remote sensing, GIS and runoff modeling. *Pakistan Journal of Meteorology*, *6*(12). 97–113.

Benn, D. I., Bolch, T., Hands, K., Gulley, J., Luckman, A., Nicholson, L. I., et al. (2012). Response of debris-covered glaciers in the Mount Everest region to recent warming, and implications for outburst flood hazards. *Earth-Science Reviews*, *114*(1–2), 156–174. https://doi.org/10.1016/j.earscirev.2012.03.008

Benn, D. I., & Lehmkuhl, F. (2000). Mass balance and equilibrium-line altitudes of glaciers in high-mountain environments. *Quaternary International*, *65*, 15–29. https://doi.org/10.1016/S1040-6182(99)00034-8

Benn, D., & Owen, L. (1998). The role of the Indian summer monsoon and the mid-latitude westerlies in Himalayan glaciation: A review and speculative discussion. *Journal of the Geological Society*, *155*, 353–363. https://doi.org/10.1144/gsjgs.155.2.0353

Benn, D. I., & Owen, L. A. (2002). Himalayan glacial sedimentary environments: A framework for reconstructing and dating former glacial extents in high mountain regions. *Quaternary International*, *97–98*, 3–26. https://doi.org/10.1016/S1040-6182(02)00048-4

Benn, D. I., Owen, L. A., Osmaston, H. A., Seltzer, G. O., Porter, S. C., & Mark, B. (2005). Reconstruction of equilibrium-line altitudes for tropical and sub-tropical glaciers. *Quaternary International*, *138*, 8–21. https://doi.org/10.1016/j.quaint.2005.02.003

Biswas, S., Coutand, I., Grujic, D., Hager, C., Stöckli, D., & Grasemann, B. (2007). Exhumation and uplift of the Shillong plateau and its influence on the eastern Himalayas: New constraints from apatite and zircon (U-Th-[Sm])/He and apatite fission track analyses. *Tectonics*, *26*(6), 1–22. https://doi.org/10.1029/2007TC002125

Böhlert, R., Gruber, S., Egli, M., Maisch, M., Brandová, D., Haeberli, W., et al. (2008). Comparison of exposure ages and spectral properties of rock surfaces in steep, high alpine rock walls of Aiguille du Midi, France. *Paper presented at 9th International Conference on Permafrost, Fairbanks, Alaska, 29 June 2008–03 July 2008* (pp. 143–148). Retrieved from https://www.zora.uzh.ch/id/eprint/2822/2/Boehlert_Exposure_Ages_2008V.pdf

Bojar, A. V., Fritz, H., Nicolescu, S., Bregar, M., & Gupta, R. (2005). Timing and mechanisms of Central Himalayan exhumation: Discriminating between tectonic and erosion processes. *Terra Nova*, *17*(5), 427–433. https://doi.org/10.1111/j.1365-3121.2005.00629.x

Bollinger, L., Henry, & Avouac, J. (2006). Mountain building in the Nepal Himalaya: Thermal and kinematic model. *Earth and Planetary Science Letters*, *244*(1–2), 58–71. https://doi.org/10.1016/j.epsl.2006.01.045

Bookhagen, B., & Burbank, D. (2006). Topography, relief and TRMM-derived rainfall variations along the Himalaya. *Geophysical Research Letters*, *33*, 105. https://doi.org/10.1029/2006GL026037

Bookhagen, B., & Burbank, D. (2010). Toward a complete Himalayan hydrological budget: Spatiotemporal distribution of snowmelt and rainfall and their impact on river discharge. *Journal of Geophysical Research*, *115*(F3), 1–25. https://doi.org/10.1029/2009JF001426

Bookhagen, B., Thiede, R., & Strecker, M. (2005a). Late quaternary intensified monsoon phases control landscape evolution in the northwest Himalaya. *Geology*, *33*(1), 149–152. https://doi.org/10.1130/G20982.1

Bookhagen, B., Thiede, R. C., & Strecker, M. R. (2005b). Abnormal monsoon years and their control on erosion and sediment flux in the high, arid northwest Himalaya. *Earth and Planetary Science Letters*, *231*(1–2), 131–146. https://doi.org/10.1016/j.epsl.2004.11.014

Boos, W. R., & Kuang, Z. (2010). Dominant control of the South Asian monsoon by orographic insulation versus plateau heating. *Nature*, *463*(7278), 218. https://doi.org/10.1038/nature08707

Braucher, R., Brown, E. T., Bourlès, D. L., & Colin, F. (2003). In situ produced ^{10}Be measurements at great depths: Implications for production rates by fast muons. *Earth and Planetary Science Letters*, *211*(3–4), 251–258. https://doi.org/10.1016/S0012-821X(03)00205-X

Brocklehurst, S. H., & Whipple, K. X. (2002). Glacial erosion and relief production in the Eastern Sierra Nevada, California. *Geomorphology*, *42*(1–2), 1–24. https://doi.org/10.1016/S0169-555X(01)00069-1

Brocklehurst, S. H., & Whipple, K. X. (2006). Assessing the relative efficiency of fluvial and glacial erosion through simulation of fluvial landscapes. *Geomorphology*, *75*(3–4), 283–299. https://doi.org/10.1016/j.geomorph.2005.07.028

Brozovic, N., Burbank, D. W., & Meigs, A. J. (1997). Climatic limits on landscape development in the northwestern Himalaya. *Science*, *276*, 571–574. https://doi.org/10.1126/science.276.5312.571

Burbank, D., Blythe, A., Putkonen, J., Pratt-Sitaula, B., Gabet, E., Oskin, M., et al. (2003). Decoupling of erosion and precipitation in the Himalayas. *Nature*, *426*, 652–655. https://doi.org/10.1038/nature02187

Cattin, R., & Avouac, J. (2000). Modeling mountain building and the seismic cycle in the Himalaya of Nepal. *Journal of Geophysical Research*, *105*(B6), 13389–13407. https://doi.org/10.1029/2000JB900032

Chmeleff, J., von Blanckenburg, F., Kossert, K., & Jakob, D. (2010). Determination of the 10Be half-life by multicollector ICP-MS and liquid scintillation counting. *Nuclear Instruments and Methods in Physics Research Section B: Beam Interactions with Materials and Atoms*, *268*(2), 192–199. https://doi.org/10.1016/j.nimb.2009.09.012

Clift, Giosan, L., Blusztajn, J., Campbell, I., Allen, C., Pringle, M., et al. (2008). Holocene erosion of the Lesser Himalaya triggered by intensified summer monsoon. *Geology*, *36*, 79–82. https://doi.org/10.1130/G24315A.1

Cossart, E., Braucher, R., Fort, M., Bourlès, D. L., & Carcaillet, J. (2008). Slope instability in relation to glacial debuttressing in alpine areas (Upper Durance catchment, southeastern France): Evidence from field data and ^{10}Be cosmic ray exposure ages. *Geomorphology*, *95*(1–2), 3–26. https://doi.org/10.1016/j.geomorph.2006.12.022

Craddock, W. H., Burbank, D. W., Bookhagen, B., & Gabet, E. J. (2007). Bedrock channel geometry along an orographic rainfall gradient in the upper Marsyandi River valley in central Nepal. *Journal of Geophysical Research*, *112*(F3). https://doi.org/10.1029/2006JF000589

de Scally, F. A. (1997). *Deriving lapse rates of slope air temperature for meltwater runoff modeling in subtropical mountains: An example from the Punjab Himalaya, Pakistan*. Mountain Research and Development. https://doi.org/10.2307/3674024

DeCelles, G., Robinson, D. M., Quade, J., Ojha, T., Garzione, C. N., Copeland, & Upreti, B. N. (2001). Stratigraphy, structure, and tectonic evolution of the Himalayan fold-thrust belt in western Nepal. *Tectonics*, *20*(4), 487–509. https://doi.org/10.1029/2000TC001226

Deeken, A., Thiede, R. C., Sobel, E. R., Hourigan, J. K., & Strecker, M. R. (2011). Exhumational variability within the Himalaya of northwest India. *Earth and Planetary Science Letters*, *305*(1–2), 103–114. https://doi.org/10.1016/j.epsl.2011.02.045

Delunel, R., Van Der Beek, P. A., Carcaillet, J., Bourlès, D. L., & Valla, P. G. (2010). Frost-cracking control on catchment denudation rates: Insights from in situ produced ^{10}Be concentrations in stream sediments (Ecrins–Pelvoux massif, French Western Alps). *Earth and Planetary Science Letters*, *293*(1–2), 72–83. https://doi.org/10.1016/j.epsl.2010.02.020

Demske, D., Tarasov, E., Wünnemann, B., & Riedel, F. (2009). Late glacial and Holocene vegetation, Indian monsoon and westerly circulation in the Trans-Himalaya recorded in the lacustrine pollen sequence from Tso Kar, Ladakh, NW India. *Palaeogeography, Palaeoclimatology, Palaeoecology*, *279*(3), 172–185. https://doi.org/10.1016/j.palaeo.2009.05.008

Derbyshire, E., Shi, Y., Li, J., Zheng, B., Li, S., & Wang, J. (1991). Quaternary glaciation of Tibet: The geological evidence. *Quaternary Science Reviews*, *10*, 485–510. https://doi.org/10.1016/0277-3791(91)90042-S

Dey, S., Thiede, R. C., Schildgen, T. F., Wittmann, H., Bookhagen, B., Scherler, D., et al. (2016). Climate-driven sediment aggradation and incision since the late Pleistocene in the NW Himalaya, India. *Earth and Planetary Science Letters*, *449*, 321–331. https://doi.org/10.1016/j.epsl.2016.05.050

Dietsch, C., Dortch, J., Reynhout, S., Owen, L., & Caffee, M. (2015). Very slow erosion rates and landscape preservation across the southwestern slope of the Ladakh Range, India. *Earth Surface Processes and Landforms*, *40*(3), 389–402. https://doi.org/10.1002/esp.3640

Dortch, J. M., Dietsch, C., Owen, L. A., Caffee, M. W., & Ruppert, K. (2011). Episodic fluvial incision of rivers and rock uplift in the Himalaya and Transhimalaya. *Journal of the Geological Society*, *168*(3), 783–804. https://doi.org/10.1144/0016-76492009-158

Dortch, J., Owen, L., & Caffee, M. (2013). Timing and climatic drivers for glaciation across semi-arid western Himalayan-Tibetan orogen. *Quaternary Science Reviews*, *78*, 188–208. https://doi.org/10.1016/j.quascirev.2013.07.025

Dortch, J. M., Owen, L. A., Haneberg, W. C., Caffee, M. W., Dietsch, C., & Kamp, U. (2009). Nature and timing of large landslides in the Himalaya and Transhimalaya of northern India. *Quaternary Science Reviews*, *28*, 1037–1056. https://doi.org/10.1016/j.quascirev.2008.05.002

Dortch, J., Owen, L., Schoenbohm, L., & Caffee, M. (2011a). Asymmetrical erosion and morphological development of the central Ladakh Range, northern India. *Geomorphology*, *135*, 167–180. https://doi.org/10.1016/j.geomorph.2011.08.014

Dunning, S. A., Rosser, N. J., McColl, S. T., & Reznichenko, N. V. (2015). Rapid sequestration of rock avalanche deposits within glaciers. *Nature Communications*, *6*(1), 1–7. https://doi.org/10.1038/ncomms8964

Edwards, M., & Richardson, A. J. (2004). Impact of climate change on marine pelagic phenology and trophic mismatch. *Nature*, *430*(7002), 881. https://doi.org/10.1038/nature02808

Eppes, M. C., & Keanini, R. (2017). Mechanical weathering and rock erosion by climate-dependent subcritical cracking. *Reviews of Geophysics*, *55*, 470–508. https://doi.org/10.1002/2017RG000557

Finkel, R., Owen, L., Barnard, P., & Caffee, M. (2003). Beryllium-10 dating of Mount Everest moraines indicates a strong monsoon influence and glacial synchroneity throughout the Himalaya. *Geology*, *31*(6), 561–564. https://doi.org/10.1130/0091-7613(2003)031<0561:BDOMEM>2.0.CO

Finlayson, D. P., Montgomery, D. R., & Hallet, B. (2002). Spatial coincidence of rapid inferred erosion with young metamorphic massifs in the Himalayas. *Geology*, *30*(3), 219–222. https://doi.org/10.1130/0091-7613(2002)030<0219:SCORIE>2.0.CO;2

Fischer, L., Amann, F., Moore, J. R., & Huggel, C. (2010). Assessment of periglacial slope stability for the 1988 Tschierva rock avalanche (Piz Morteratsch, Switzerland). *Engineering Geology*, *116*(1–2), 32–43. https://doi.org/10.1016/j.enggeo.2010.07.005

Fischer, L., Kääb, A., Huggel, C., & Noetzli, J. (2006). Geology, glacier retreat and permafrost degradation as controlling factors of slope instabilities in a high-mountain rock wall: The Monte Rosa east face. *Natural Hazards and Earth System Sciences*, *6*(5), 761–772. https://doi.org/10.5194/nhess-6-761-2006

Fischer, L., Purves, R. S., Huggel, C., Noetzli, J., & Haeberli, W. (2012). On the influence of topographic, geological and cryospheric factors on rock avalanches and rockfalls in high-mountain areas. *Natural Hazards and Earth System Sciences*, *12*(1), 241. https://doi.org/10.5194/nhess-12-241-2012

Fleitmann, D., Burns, S. J., Mudelsee, M., Neff, U., Kramers, J., Mangini, A., & Matter, A. (2003). Holocene forcing of the Indian monsoon recorded in a stalagmite from southern Oman. *Science*, *300*, 1737–1739. https://doi.org/10.1126/science.1083130

Foster, D., Brocklehurst, S. H., & Gawthorpe, R. L. (2008). Small valley glaciers and the effectiveness of the glacial buzzsaw in the northern Basin and Range, USA. *Geomorphology*, *102*(3–4), 624–639. https://doi.org/10.1016/j.geomorph.2008.06.009

Frank, W., Hoinkes, G., Miller, C., Purtscheller, F., Richter, W., & Thöni, M. (1973). Relations between metamorphism and orogeny in a typical section of the Indian Himalayas. *Tschermaks mineralogische und petrographische Mitteilungen*, *20*(4), 303–332. https://doi.org/10.1007/BF01081339

Gabet, E. J., Burbank, D. W., Pratt-Sitaula, B., Putkonen, J., & Bookhagen, B. (2008). Modern erosion rates in the High Himalayas of Nepal. *Earth and Planetary Science Letters*, *267*(3-4), 482–494. https://doi.org/10.1016/j.epsl.2007.11.059

Gadgil, S. (2003). The Indian monsoon and its variability. *Annual Review of Earth and Planetary Sciences*, *31*(1), 429–467. https://doi.org/10.1146/annurev.earth.31.100901.141251

Gale, S. J., & Hoare, G. (1991). *Quaternary sediments: Petrographic methods for the study of unlithified rocks*. Chichester: Wiley.

Gallach, X., Ravanel, L., Egli, M., Brandova, D., Schaepman, M., Christl, M., et al. (2018). Timing of rockfalls in the Mont Blanc massif (Western Alps): Evidence from surface exposure dating with cosmogenic ^{10}Be. *Landslides*, *15*(10), 1991–2000. https://doi.org/10.1007/s10346-018-0999-8

Gasparini, N. M., & Whipple, K. X. (2014). Diagnosing climatic and tectonic controls on topography: Eastern flank of the northern Bolivian Andes. *Lithosphere*, *6*(4), 230–250. https://doi.org/10.1130/L322.1

Gibson, M. J., Glasser, N. F., Quincey, D. J., Mayer, C., Rowan, A. V., & Irvine-Fynn, T. D. (2017). Temporal variations in supraglacial debris distribution on Baltoro Glacier, Karakoram between 2001 and 2012. *Geomorphology*, *295*, 572–585. https://doi.org/10.1016/j.geomorph.2017.08.012

Godard, V., Bourlès, D. L., Spinabella, F., Burbank, D. W., Bookhagen, B., Fisher, G. B., et al. (2014). Dominance of tectonics over climate in Himalayan denudation. *Geology*, *42*(3), 243–246. https://doi.org/10.1130/G35342.1

Godard, V., Cattin, R., & Lavé, J. (2004). Numerical modeling of mountain building: Interplay between erosion law and crustal rheology. *Geophysical Research Letters*, *31*(23), 1–5. https://doi.org/10.1029/2004GL021006

Goodsell, B., Hambrey, M. J., & Glasser, N. F. (2005). Debris transport in a temperate valley glacier: Haut Glacier d'Arolla, Valais, Switzerland. *Journal of Glaciology*, *51*(172), 139–146. https://doi.org/10.3189/172756505781829647

Granger, D. E., Kirchner, J. W., & Finkel, R. (1996). Spatially averaged long-term erosion rates measured from in situ-produced cosmogenic nuclides in alluvial sediment. *The Journal of Geology*, *104*(3), 249–257. https://doi.org/10.1086/629823

Gruber, S., & Haeberli, W. (2007). Permafrost in steep bedrock slopes and its temperature-related destabilization following climate change. *Journal of Geophysical Research*, *112*(F2), 1–10. https://doi.org/10.1029/2006JF000547

Grujic, D., Coutand, I., Bookhagen, B., Bonnet, S., Blythe, A., & Duncan, C. (2006). Climatic forcing of erosion, landscape, and tectonics in the Bhutan Himalayas. *Geology*, *34*(10), 801–804. https://doi.org/10.1130/G22648.1

Gupta, A. K., Anderson, D. M., & Overpeck, J. T. (2003). Abrupt changes in the Asian southwest monsoon during the Holocene and their links to North Atlantic Ocean. *Nature*, *421*, 354–357. https://doi.org/10.1038/nature01340

Haeberli, W., Schaub, Y., & Huggel, C. (2017). Increasing risks related to landslides from degrading permafrost into new lakes in de-glaciating mountain ranges. *Geomorphology*, *293*, 405–417. https://doi.org/10.1016/j.geomorph.2016.02.009

Hales, T. C., & Roering, J. J. (2005). Climate-controlled variations in scree production, Southern Alps, New Zealand. *Geology*, *33*(9), 701–704. https://doi.org/10.1130/G21528.1

Hales, T. C., & Roering, J. J. (2007). Climatic controls on frost cracking and implications for the evolution of bedrock landscapes. *Journal of Geophysical Research*, *112*(F2), 1–14. https://doi.org/10.1029/2006JF000616

Hallet, B., Walder, J. S., & Stubbs, C. W. (1991). Weathering by segregation ice growth in microcracks at sustained subzero temperatures: Verification from an experimental study using acoustic emissions. *Permafrost and Periglacial Processes*, *2*(4), 283–300. https://doi.org/10.1002/ppp.3430020404

Hambrey, M. J., Quincey, D. J., Glasser, N. F., Reynolds, J. M., Richardson, S. J., & Clemmens, S. (2008). Sedimentological, geomorphological and dynamic context of debris-mantled glaciers, Mount Everest (Sagarmatha) region, Nepal. *Quaternary Science Reviews*, *27*(25–26), 2361–2389. https://doi.org/10.1016/j.quascirev.2008.08.010

Hasnain, S. I. (1996). Factors controlling suspended sediment transport in Himalayan glacier meltwaters. *Journal of Hydrology*, *181*(1–4), 49–62. https://doi.org/10.1016/0022-1694(95)02917-6

Hedrick, K., Seong, Y., Owen, L., Caffee, M., & Dietsch, C. (2011). Toward defining the transition in style and timing of Quaternary glaciation between the monsoon-influenced Greater Himalaya and the semi-arid Transhimalaya of Northern India. *Quaternary International*, *236*, 21–33. https://doi.org/10.1016/j.quaint.2010.07.023

Heimsath, A. M., & McGlynn, R. (2008). Quantifying periglacial erosion in the Nepal high Himalaya. *Geomorphology*, *97*(1–2), 5–23. https://doi.org/10.1016/j.geomorph.2007.02.046

Herman, F., Copeland, Avouac, J., Bollinger, L., Mahéo, G., Le Fort, et al. (2010). Exhumation, crustal deformation, and thermal structure of the Nepal Himalaya derived from the inversion of thermochronological and thermobarometric data and modeling of the topography. *Journal of Geophysical Research*, *115*(B6), 1–38. https://doi.org/10.1029/2008JB006126

Hewitt, K. (2002). Altitudinal organization of Karakoram geomorphic processes and depositional environments. *Himalaya to the sea* (pp. 118–133). Routledge.

Hodges, K. V. (2000). Tectonics of the Himalaya and southern Tibet from two perspectives. *Geological Society of America Bulletin*, *112*(3), 324–350. https://doi.org/10.1130/0016-7606(2000)112<324:TOTHAS>2.0.CO;2

Hodges, K. V., Wobus, C., Ruhl, K., Schildgen, T., & Whipple, K. (2004). Quaternary deformation, river steepening, and heavy precipitation at the front of the Higher Himalayan ranges. *Earth and Planetary Science Letters*, *220*(3–4), 379–389. https://doi.org/10.1016/S0012-821X(04)00063-9

Hovius, N., Stark, C., Hao-Tsu, C., & Jiun-Chuan, L. (2000). Supply and removal of sediment in a landslide-dominated mountain belt: Central Range, Taiwan. *The Journal of Geology*, *108*(1), 73–89. https://doi.org/10.1086/314387

Immerzeel, W. W., Kraaijenbrink, P. D., Shea, J. M., Shrestha, A. B., Pellicciotti, F., Bierkens, M. F., & de Jong, S. M. (2014). High-resolution monitoring of Himalayan glacier dynamics using unmanned aerial vehicles. *Remote Sensing of Environment*, *150*, 93–103. https://doi.org/10.1016/j.rse.2014.04.025

Iverson, R. M. (2000). Landslide triggering by rain infiltration. *Water Resources Research*, *36*(7), 1897–1910. https://doi.org/10.1029/2000WR900090

Jain, A. K., Kumar, D., Singh, S., Kumar, A., & Lal, N. (2000). Timing, quantification and tectonic modeling of Pliocene–Quaternary movements in the NW Himalaya: Evidence from fission track dating. *Earth and Planetary Science Letters*, *179*(3–4), 437–451. https://doi.org/10.1016/S0012-821X(00)00133-3

Jones, D., Lister, D. H., Osborn, T. J., Harpham, C., Salmon, M., & Morice, C. (2012). Hemispheric and large-scale land-surface air temperature variations: An extensive revision and an update to 2010. *Journal of Geophysical Research*, *117*(D5), 1–29. https://doi.org/10.1029/2011JD017139

Kattel, D. B., Yao, T., Yang, K., Tian, L., Yang, G., & Joswiak, D. (2013). Temperature lapse rate in complex mountain terrain on the southern slope of the central Himalayas. *Theoretical and Applied Climatology*, *113*(3–4), 671–682. https://doi.org/10.1007/s00704-012-0816-6

Kirchner, J. W., Finkel, R. C., Riebe, C. S., Granger, D. E., Clayton, J. L., King, J. G., & Megahan, W. F. (2001). Mountain erosion over 10 yr, 10 ky, and 10 my time scales. *Geology*, *29*(7), 591–594. https://doi.org/10.1130/0091-7613(2001)029<0591:MEOYKY>2.0.CO;2

Kirstein, L. A., Foeken, J. T., Van Der Beek, Stuart, F. M., & Phillips, R. J. (2009). Cenozoic unroofing history of the Ladakh Batholith, western Himalaya, constrained by thermochronology and numerical modeling. *Journal of the Geological Society*, *166*(4), 667–678. https://doi.org/10.1144/0016-76492008-107

Kirstein, L. A., Sinclair, H., Stuart, F. M., & Dobson, K. (2006). Rapid early Miocene exhumation of the Ladakh batholith, western Himalaya. *Geology*, *34*(12), 1049–1052. https://doi.org/10.1130/G22857A.1

Korschinek, G., Bergmaier, A., Faestermann, T., Gerstmann, U. C., Knie, K., Rugel, G., et al. (2010). A new value for the half-life of ^{10}Be by heavy-ion elastic recoil detection and liquid scintillation counting. *Nuclear Instruments and Methods in Physics Research Section B: Beam Interactions with Materials and Atoms*, *268*(2), 187–191. https://doi.org/10.1016/j.nimb.2009.09.020

Krautblatter, M., & Moore, J. R. (2014). Rock slope instability and erosion: toward improved process understanding. *Earth Surface Processes and Landforms*, *39*(9), 1273–1278. https://doi.org/10.1002/esp.3578

Kumar, A., Gupta, A. K., Bhambri, R., Verma, A., Tiwari, S. K., & Asthana, A. K. L. (2018). Assessment and review of hydro meteorological aspects for cloudburst and flash flood events in the third pole region (Indian Himalaya). *Polar Science*, *18*, 5–20. https://doi.org/10.1016/j.polar.2018.08.004

Lal, D. (1991). Cosmic ray labeling of erosion surfaces: in situ nuclide production rates and erosion models. *Earth and Planetary Science Letters*, *104*, 429–439. https://doi.org/10.1016/0012-821X(91)90220-C

Lang, T. J., & Barros, A. (2004). Winter storms in the central Himalayas. *Journal of the Meteorological Society of Japan. Series II*, *82*(3), 829–844. https://doi.org/10.2151/jmsj.2004.829

Lavé, J., & Avouac, J. (2000). Active folding of fluvial terraces across the Siwaliks Hills, Himalayas of central Nepal. *Journal of Geophysical Research*, *105*(B3), 5735–5770. https://doi.org/10.1029/1999JB900292

Lavé, J., & Avouac, J. (2001). Fluvial incision and tectonic uplift across the Himalayas of central Nepal. *Journal of Geophysical Research*, *106*(B11), 26561–26591. https://doi.org/10.1029/2001JB000359

Leith, K., Moore, J., Amann, F., & Loew, S. (2010). Slope failure induced by post-glacial ex-tensional fracturing in the matter and Saas Valleys, Switzerland. *Geophysical Research Abstracts*, *12*, 4599.

Liu, X., & Dong, B. (2013). Influence of the Tibetan plateau uplift on the Asian monsoon-arid environment evolution. *Chinese Science Bulletin*, *58*(34), 4277–4291. https://doi.org/10.1007/s11434-013-5987-8

Lukas, S., Graf, A., Coray, S., & Schlüchter, C. (2012). Genesis, stability and preservation potential of large lateral moraines of Alpine valley glaciers–toward a unifying theory based on Findelengletscher, Switzerland. *Quaternary Science Reviews*, *38*, 27–48. https://doi.org/10.1016/j.quascirev.2012.01.022

Lupker, M., Blard, H., Lave, J., France-Lanord, C., Leanni, L., Puchol, N., (2012). ^{10}Be-derived Himalayan denudation rates and sediment budgets in the Ganga basin. *Earth and Planetary Science Letters*, *333*, 146–156. https://doi.org/10.1016/j.epsl.2012.04.020

Lupker, M., France-Lanord, C., Galy, V., Lavé, J., & Kudrass, H. (2013). Increasing chemical weathering in the Himalayan system since the Last Glacial Maximum. *Earth and Planetary Science Letters*, *365*, 243–252. https://doi.org/10.1016/j.epsl.2013.01.038

MacGregor, K. R., Anderson, R. S., & Waddington, E. D. (2009). Numerical modeling of glacial erosion and headwall processes in alpine valleys. *Geomorphology*, *103*(2), 189–204. https://doi.org/10.1016/j.geomorph.2008.04.022

Martin, L., Blard, Balco, G., & Laurent, V. (2017). The CREp program and the ICE-D production rate calibration database: A fully parameterizable and updated online tool to compute cosmic-ray exposure ages. *Quaternary Geochronology*, *38*, 25–49. https://doi.org/10.1016/j.quageo.2016.11.006

Matsuoka, N. (2001). Microgelivation versus macrogelivation: toward bridging the gap between laboratory and field frost weathering. *Permafrost and Periglacial Processes*, *12*(3), 299–313. https://doi.org/10.1002/ppp.393

Matsuoka, N., & Sakai, H. (1999). Rockfall activity from an alpine cliff during thawing periods. *Geomorphology*, *28*(3–4), 309–328. https://doi.org/10.1016/S0169-555X(98)00116-0

McColl, S. T. (2012). Paraglacial rock-slope stability. *Geomorphology*, *153*, 1–16. https://doi.org/10.1016/j.geomorph.2012.02.015

McColl, S. T., & Davies, T. R. (2013). Large ice-contact slope movements: glacial buttressing, deformation and erosion. *Earth Surface Processes and Landforms*, *38*(10), 1102–1115. https://doi.org/10.1002/esp.3346

Meunier, P., Hovius, N., & Haines, J. A. (2008). Topographic site effects and the location of earthquake induced landslides. *Earth and Planetary Science Letters*, *275*(3–4), 221–232. https://doi.org/10.1016/j.epsl.2008.07.020

Miller, C., Klötzli, U., Frank, W., Thöni, M., & Grasemann, B. (2000). Proterozoic crustal evolution in the NW Himalaya (India) as recorded by circa 1.80 Ga mafic and 1.84 Ga granitic magmatism. *Precambrian Research*, *103*, 191–206. https://doi.org/10.1016/S0301-9268(00)00091-7

Miller, C., Thöni, M., Frank, W., Grasemann, B., Klötzli, U., Guntli, & Draganits, E. (2001). The early Palaeozoic magmatic event in the Northwest Himalaya, India: Source, tectonic setting and age of emplacement. *Geological Magazine*, *138*(3), 237–251. https://doi.org/10.1017/S0016756801005283

Mitchell, S. G., & Montgomery, D. R. (2006). Influence of a glacial buzzsaw on the height and morphology of the Cascade Range in central Washington State, USA. *Quaternary Research*, *65*(1), 96–107. https://doi.org/10.1016/j.yqres.2005.08.018

Mölg, T., Maussion, F., & Scherler, D. (2014). Mid-latitude westerlies as a driver of glacier variability in monsoonal High Asia. *Nature Climate Change*, *4*(1), 68. https://doi.org/10.1038/nclimate2055

Moon, S., Perron, J. T., Martel, S. J., Holbrook, W. S., & Clair, J. (2017). A model of three-dimensional topographic stresses with implications for bedrock fractures, surface processes, and landscape evolution. *Journal of Geophysical Research: Earth Surface*, *122*(4), 823–846. https://doi.org/10.1002/2016JF004155

Moore, R. D., Fleming, S. W., Menounos, B., Wheate, R., Fountain, A., Stahl, K., et al. (2009). Glacier change in western North America: Influences on hydrology, geomorphic hazards and water quality. *Hydrological Processes*, *23*(1), 42–61. https://doi.org/10.1002/hyp.7162

Murari, M. K., Owen, L. A., Dortch, J. M., Caffee, M. W., Dietsch, C., Fuchs, M., et al. (2014). Timing and climatic drivers for glaciation across monsoon-influenced regions of the Himalayan–Tibetan orogen. *Quaternary Science Reviews*, *88*, 159–182. https://doi.org/10.1016/j.quascirev.2014.01.013

Muzikar, P. (2008). Cosmogenic nuclide concentrations in episodically eroding surfaces: Theoretical results. *Geomorphology*, *97*(3–4), 407–413. https://doi.org/10.1016/j.geomorph.2007.08.020

Nagai, H., Fujita, K., Nuimura, T., & Sakai, A. (2013). Southwest-facing slopes control the formation of debris-covered glaciers in the Bhutan Himalaya. *The Cryosphere*, *7*(4), 1303. https://doi.org/10.5194/tc-7-1303-2013

Naylor, S., & Gabet, E. J. (2007). Valley asymmetry and glacial versus nonglacial erosion in the Bitterroot Range, Montana, USA. *Geology*, *35*(4), 375–378. https://doi.org/10.1130/G23283A.1

Nishiizumi, K., Winterer, E. L., Kohl, C. P., Klein, J., Middleton, R., Lal, D., & Arnold, J. R. (1989). Cosmic ray production rates of ^{10}Be and ^{26}Al in quartz from glacially polished rocks. *Journal of Geophysical Research*, *94*(B12), 17907–17915. https://doi.org/10.1029/JB094iB12p17907

Orr, E., Owen, L., Murari, M., Saha, S., & Caffee, M. (2017). The timing and extent of Quaternary glaciation of Stok, northern Zanskar Range, Transhimalaya, of northern India. *Geomorphology*, *284*, 142–155. https://doi.org/10.1016/j.geomorph.2016.05.031

Orr, E. N., Owen, L. A., Saha, S., & Caffee, M. W. (2019). Rates of rockwall slope erosion in the upper Bhagirathi catchment, Garhwal Himalaya. *Earth Surface Processes and Landforms*, *44*(15), 3108–3127. https://doi.org/10.1002/esp.4720

Orr, E. N., Owen, L. A., Saha, S., Caffee, M. W., & Murari, M. K. (2018). Quaternary glaciation of the Lato Massif, Zanskar Range of the NW Himalaya. *Quaternary Science Reviews*, *183*, 140–156. https://doi.org/10.1016/j.quascirev.2018.01.005

Osborn, T. J., & Jones, P. (2014). The CRUTEM4 land-surface air temperature data set: Construction, previous versions and dissemination via Google Earth. *Earth System Science Data*, *6*(1), 61–68. https://doi.org/10.5194/essd-6-61-2014

Oskin, M., & Burbank, D. W. (2005). Alpine landscape evolution dominated by cirque retreat. *Geology*, *33*(12), 933–936. https://doi.org/10.1130/G21957.1

Osmaston, H. (2005). Estimates of glacier equilibrium line altitudes by the Area× Altitude, the Area× Altitude Balance Ratio and the Area× Altitude Balance Index methods and their validation. *Quaternary International*, *138*, 22–31. https://doi.org/10.1016/j.quaint.2005.02.004

Ouimet, W. B., Whipple, K. X., & Granger, D. E. (2009). Beyond threshold hillslopes: Channel adjustment to base-level fall in tectonically active mountain ranges. *Geology*, *37*(7), 579–582. https://doi.org/10.1130/G30013A.1

Owen, L., Caffee, M., Bovard, K., Finkel, R., & Sharma, M. (2006). Terrestrial cosmogenic nuclide surface exposure dating of the oldest glacial successions in the Himalayan orogen: Ladakh Range, northern India. *Geological Society of America Bulletin*, *118*(3–4), 383–392. https://doi.org/10.1130/B25750.1

Owen, L. A., Caffee, M. W., Finkel, R. C., & Seong, B. S. (2008). Quaternary glaciation of the Himalayan–Tibetan orogen. *Journal of Quaternary Science*, *23*, 513–532. https://doi.org/10.1002/jqs.1203

Owen, L., & Dortch, J. (2014). Nature and timing of Quaternary glaciation in the Himalayan-Tibetan orogen. *Quaternary Science Reviews*, *88*, 14–54. https://doi.org/10.1016/j.quascirev.2013.11.016

Owen, L. A., & Sharma, M. C. (1998). Rates and magnitudes of paraglacial fan formation in the Garhwal Himalaya: Implications for landscape evolution. *Geomorphology*, *26*(1–3), 171–184. https://doi.org/10.1016/S0169-555X(98)00057-9

Östrem, G. (1959). Ice melting under a thin layer of moraine, and the existence of ice cores in moraine ridges. *Geografiska Annaler*, *41*(4), 228–230. https://doi.org/10.1080/20014422.1959.11907953

Patel, L. K., Sharma, P., Fathima, T. N., & Thamban, M. (2018). Geospatial observations of topographical control over the glacier retreat, Miyar basin, Western Himalaya, India. *Environmental Earth Sciences*, *77*(5), 190. https://doi.org/10.1007/s12665-018-7379-5

Portenga, E. W., & Bierman, R. (2011). Understanding Earth's eroding surface with ^{10}Be. *Geological Society of America Today*, *21*(8), 4–10.

Portenga, E. W., Bierman, R., Duncan, C., Corbett, L. B., Kehrwald, N. M., & Rood, D. H. (2015). Erosion rates of the Bhutanese Himalaya determined using in situ-produced ^{10}Be. *Geomorphology*, *233*, 112–126. https://doi.org/10.1016/j.geomorph.2014.09.027

Pratap, B., Dobhal, D., Bhambri, R., & Mehta, M. (2013). Near-surface temperature lapse rate in Dokriani Glacier catchment, Garhwal Himalaya, India. *Himalayan Geology*, *34*, 183–186.

Puchol, N., Lavé, J., Lupker, M., Blard, P. H., Gallo, F., & France-Lanord, C., & ASTER Team (2014). Grain-size dependent concentration of cosmogenic ^{10}Be and erosion dynamics in a landslide-dominated Himalayan watershed. *Geomorphology*, *224*, 55–68. https://doi.org/10.1016/j.geomorph.2014.06.019

Qiang, X. K., Li, Z. X., Powell, C. M., & Zheng, H. B. (2001). Magnetostratigraphic record of the Late Miocene onset of the East Asian monsoon, and Pliocene uplift of northern Tibet. *Earth and Planetary Science Letters*, *187*(1–2), 83–93. https://doi.org/10.1016/S0012-821X(01)00281-3

Rajendran, K., Rajendran, C., Jain, S. K., Murty, C. V. R., & Arlekar, J. N. (2000). The Chamoli earthquake, Garhwal Himalaya: Field observations and implications for seismic hazard. *Current Science*, *78*(1), 45–51.

Regmi, D., & Watanabe, T. (2009). Rockfall activity in the Kangchenjunga area, Nepal Himalaya. *Permafrost and Periglacial Processes*, *20*(4), 390–398. https://doi.org/10.1002/ppp.664

Robert, X., Van Der Beek, Braun, J., Perry, C., & Mugnier, J. L. (2011). Control of detachment geometry on lateral variations in exhumation rates in the Himalaya: Insights from low-temperature thermochronology and numerical modeling. *Journal of Geophysical Research*, *116*(B5), 1–22. https://doi.org/10.1029/2010JB007893

Sadler, M., & Jerolmack, D. J. (2014). Scaling laws for aggradation, denudation and progradation rates: the case for time-scale invariance at sediment sources and sinks. *Geological Society, London, Special Publications*, *404*, 404–407. https://doi.org/10.1144/SP404.7

Sagredo, E. A., & Lowell, T. V. (2012). Climatology of Andean glaciers: A framework to understand glacier response to climate change. *Global and Planetary Change*, *86*, 101–109. https://doi.org/10.1016/j.gloplacha.2012.02.010

Saha, S., Owen, L. A., Orr, E. N., & Caffee, M. W. (2018). Timing and nature of Holocene glacier advances at the northwestern end of the Himalayan-Tibetan orogen. *Quaternary Science Reviews*, *187*, 177–202. https://doi.org/10.1016/j.quascirev.2018.03.009

Saha, S., Owen, L. A., Orr, E. N., & Caffee, M. W. (2019). High-frequency Holocene glacier fluctuations in the Himalayan-Tibetan orogen. *Quaternary Science Reviews*, *220*, 372–400. https://doi.org/10.1016/j.quascirev.2019.07.021

Sanchez, G., Rolland, Y., Corsini, M., Braucher, R., Bourlès, D., Arnold, M., & Aumaître, G. (2009). Relationships between tectonics, slope instability and climate change: Cosmic ray exposure dating of active faults, landslides and glacial surfaces in the SW Alps. *Geomorphology*, *117*, 1–13. https://doi.org/10.1016/j.geomorph.2009.10.019

Sanders, J. W., Cuffey, K. M., MacGregor, K. R., & Collins, B. D. (2013). The sediment budget of an alpine cirque. *Geological Society of Ameica Bulletin*, *125*(1–2), 229–248. https://doi.org/10.1130/B30688.1

Sanders, J. W., Cuffey, K. M., Moore, J. R., MacGregor, K. R., & Kavanaugh, J. L. (2012). Periglacial weathering and headwall erosion in cirque glacier bergschrunds. *Geology*, *40*(9), 779–782. https://doi.org/10.1130/G33330.1

Sarr, A. C., Mugnier, J. L., Abrahami, R., Carcaillet, J., & Ravanel, L. (2019). Sidewall erosion: Insights from in situ-produced ^{10}Be concentrations measured on supraglacial clasts (Mont Blanc massif, France). *Earth Surface Processes and Landforms*, *44*(10), 1930–1944. https://doi.org/10.1002/esp.4620

Schelling, D., & Arita, K. (1991). Thrust tectonics, crustal shortening, and the structure of the far-eastern Nepal Himalaya. *Tectonics*, *10*(5), 851–862. https://doi.org/10.1029/91TC01011

Scherler, D., Bookhagen, B., & Strecker, M. R. (2011). Hillslope-glacier coupling: The interplay of topography and glacial dynamics in High Asia. *Journal of Geophysical Research*, *116*(F2), 1–21. https://doi.org/10.1029/2010JF001751

Scherler, D., Bookhagen, B., & Strecker, M. R. (2014). Tectonic control on ^{10}Be-derived erosion rates in the Garhwal Himalaya, India. *Journal of Geophysical Research: Earth Surface*, *119*(2), 83–105. https://doi.org/10.1002/2013JF002955

Scherler, D., Bookhagen, B., Wulf, H., Preusser, F., & Strecker, M. R. (2015). Increased late Pleistocene erosion rates during fluvial aggradation in the Garhwal Himalaya, northern India. *Earth and Planetary Science Letters*, *428*, 255–266. https://doi.org/10.1016/j.epsl.2015.06.034

Scherler, D., & Egholm, D. L. (2020). Production and transport of supraglacial debris: Insights from cosmogenic ^{10}Be and numerical modeling, Chhota Shigri Glacier, Indian Himalaya. *Journal of Geophysical Research: Earth Surface*, *125*(10), e2020JF005586. https://doi.org/10.1029/2020JF005586

Schlup, M., Carter, A., Cosca, M., & Steck, A. (2003). Exhumation history of eastern Ladakh revealed by 40Ar/39Ar and fission-track ages: the Indus River-Tso Morari transect, NW Himalayas. *Journal of the Geological Society*, *160*, 385–399. https://doi.org/10.1144/0016-764902-084

Schlup, M., Steck, A., Carter, A., Cosca, M., Epard, J. L., & Hunziker, J. (2011). Exhumation history of the NW Indian Himalaya revealed by fission track and 40Ar/39Ar ages. *Journal of Asian Earth Sciences*, *40*(1), 334–350. https://doi.org/10.1016/j.jseaes.2010.06.008

Schroder, J. F., Bishop, M. P., Copland, L., & Sloan, V. F. (2000). Debris-covered glaciers and rock glaciers in the Nanga Parbat Himalaya, Pakistan. *Geografiska Annaler: Series A*, *82A*, 17–31. https://doi.org/10.1111/j.0435-3676.2000.00108.x

Seaby, R.M., & Henderson, P.A. (2014). In *Community analysis package; version 5.3. 3.472*. Pisces Conservation Ltd, Pennington. Retrieved from www.pisces-conservation.com

Searle, M. (1986). Structural evolution and sequence of thrusting in the High Himalayan, Tibetan-Tethys and Indus suture zones of Zanskar and Ladakh, Western Himalaya. *Journal of Structural Geology*, *8*(8), 923–936. https://doi.org/10.1016/0191-8141(86)90037-4

Searle, M. P., Elliott, J. R., Phillips, R. J., & Chung, S. L. (2011). Crustal–lithospheric structure and continental extrusion of Tibet. *Journal of the Geological Society*, *168*(3), 633–672. https://doi.org/10.1144/0016-76492010-139

Searle, M., & Fryer, B. J. (1986). Garnet, tourmaline and muscovite-bearing leucogranites, gneisses and migmatites of the Higher Himalayas from Zanskar, Kulu, Lahoul and Kashmir. *Geological Society, London, Special Publications*, *19*(1), 185–201. https://doi.org/10.1144/GSL.SP.1986.019.01.10

Searle, M. P., Noble, S. R., Hurford, A. J., & Rex, D. C. (1999). Age of crustal melting, emplacement and exhumation history of the Shivling leucogranite, Garhwal Himalaya. *Geological Magazine*, *136*(5), 513–525. https://doi.org/10.1017/S0016756899002885

Searle, M., Parrish, R., Hodges, K., Hurford, A., Ayres, M., & Whitehouse, M. (1997). Shisha Pangma leucogranite, south Tibetan Himalaya: Field relations, geochemistry, age, origin, and emplacement. *Journal of Geology*, *150*, 295–317. https://doi.org/10.1086/515924

Seong, Y. B., Owen, L. A., Caffee, M. W., Kamp, U., Bishop, M. P., Bush, A., et al. (2009). Rates of basin-wide rockwall retreat in the K2 region of the Central Karakoram defined by terrestrial cosmogenic nuclide ^{10}Be. *Geomorphology*, *107*(3–4), 254–262. https://doi.org/10.1016/j.geomorph.2008.12.014

Sharma, P., Bourgeois, M., Elmore, D., Granger, D., Lipschutz, M. E., Ma, X., et al. (2000). PRIME lab AMS performance, upgrades and research applications. *Nuclear Instruments And Methods In Physics Research B*, *172*, 112–123. https://doi.org/10.1016/S0168-583X(00)00132-4

Sharma, S., Shukla, A. D., Bartarya, S. K., Marh, B. S., & Juyal, N. (2017). The Holocene floods and their affinity to climatic variability in the western Himalaya, India. *Geomorphology*, *290*, 317–334. https://doi.org/10.1016/j.geomorph.2017.04.030

Small, E. E., & Anderson, R. S. (1998). Pleistocene relief production in Laramide mountain ranges, western United States. *Geology*, *26*(2), 123–126. https://doi.org/10.1130/0091-7613(1998)026<0123:PRPILM>2.3.CO;2

Small, E. E., Anderson, R. S., Repka, J. L., & Finkel, R. (1997). Erosion rates of alpine bedrock summit surfaces deduced from in situ ^{10}Be and ^{26}Al. *Earth and Planetary Science Letters*, *150*(3–4), 413–425. https://doi.org/10.1016/S0012-821X(97)00092-7

Solomina, O. N., Bradley, R. S., Hodgson, D. A., Ivy-Ochs, S., Jomelli, V., Mackintosh, A. N., et al. (2015). Holocene glacier fluctuations. *Quaternary Science Reviews*, *111*, 9–34. https://doi.org/10.1016/j.quascirev.2014.11.018

Solomina, O. N., Bradley, R. S., Jomelli, V., Geirsdottir, A., Kaufman, D. S., Koch, J., et al. (2016). Glacier fluctuations during the past 2000 years. *Quaternary Science Reviews*, *149*, 61–90. https://doi.org/10.1016/j.quascirev.2016.04.008

Sorkhabi, R. B., Stump, E., Foland, K. A., & Jain, A. K. (1996). Fission-track and ^{40}Ar^{39}Ar evidence for episodic denudation of the Gangotri granites in the Garhwal Higher Himalaya, India. *Tectonophysics*, *260*(1–3), 187–199. https://doi.org/10.1016/0040-1951(96)00083-2

Srivastava, P., & Mitra, G. (1994). Thrust geometries and deep structure of the outer and lesser Himalaya, Kumaon and Garhwal (India): Implications for evolution of the Himalayan fold-and-thrust belt. *Tectonics*, *13*(1), 89–109. https://doi.org/10.1029/93TC01130

Steck, A., Epard, J., Vannay, J., Hunziker, J., Girard, M., Morard, A., & Robyr, M. (1998). Geological transect across the Tso Morari and Spiti areas- the nappe structures of the Tethys Himalayas. *Eclogae Geologicae Helvetiae*, *91*, 103–121.

Strahler, A. N. (1952). Hypsometric (area-altitude) analysis of erosional topography. *Geological Society of America Bulletin*, *63*(11), 1117–1142. https://doi.org/10.1130/0016-7606(1952)63[1117:HAAOET]2.0.CO

Streule, M. J., Searle, M., Waters, D. J., & Horstwood, M. S. (2010). Metamorphism, melting, and channel flow in the Greater Himalayan Sequence and Makalu leucogranite: Constraints from thermobarometry, metamorphic modeling, and U-Pb geochronology. *Tectonics*, *29*, 5. https://doi.org/10.1029/2009TC002533

Su, Z., & Shi, Y. (2002). Response of monsoonal temperate glaciers to global warming since the Little Ice Age. *Quaternary International*, *97*, 123–131. https://doi.org/10.1016/S1040-6182(02)00057-5

Team, RC (2018). *R: A language and environment for statistical computing*. Austria: Vienna: R Foundation for Statistical Computing.

Thayyen, R. J., Gergan, J. T., & Dobhal, D. (2005). Slope lapse rates of temperature in Din Gad (Dokriani glacier) catchment, Garhwal Himalaya, India. *Bulletin of Glaciological Research*, *22*, 31–37.

Thiede, R. C., Arrowsmith, J. R., Bookhagen, B., McWilliams, M. O., Sobel, E. R., & Strecker, M. R. (2005). From tectonically to erosionally controlled development of the Himalayan orogen. *Geology*, *33*(8), 689–692. https://doi.org/10.1130/G21483AR.1

Thiede, R. C., Arrowsmith, J. R., Bookhagen, B., McWilliams, M., Sobel, E. R., & Strecker, M. R. (2006). Dome formation and extension in the Tethyan Himalaya, Leo Pargil, northwest India. *Geological Society of America Bulletin*, *118*(5–6), 635–650. https://doi.org/10.1130/B25872.1

Thiede, R. C., Bookhagen, B., Arrowsmith, J. R., Sobel, E. R., & Strecker, M. R. (2004). Climatic control on rapid exhumation along the Southern Himalayan Front. *Earth and Planetary Science Letters*, *222*(3–4), 791–806. https://doi.org/10.1016/j.epsl.2004.03.015

Thiede, R. C., & Ehlers, T. A. (2013). Large spatial and temporal variations in Himalayan denudation. *Earth and Planetary Science Letters*, *371*, 278–293. https://doi.org/10.1016/j.epsl.2013.03.004

Thiede, R. C., Ehlers, T. A., Bookhagen, B., & Strecker, M. R. (2009). Erosional variability along the northwest Himalaya. *Journal of Geophysical Research*, *114*(F1), 1–19. https://doi.org/10.1029/2008JF001010

Thomas, E. K., Huang, Y., Clemens, S. C., Colman, S. M., Morrill, C., Wegener, & Zhao, J. (2016). Changes in dominant moisture sources and the consequences for hydroclimate on the northeastern Tibetan Plateau during the past 32 kyr. *Quaternary Science Reviews*, *131*, 157–167. https://doi.org/10.1016/j.quascirev.2015.11.003

Thompson, L. O., Yao, T., Davis, M. E., Henderson, K. A., Mosley-Thompson, E., Lin, N., et al. (1997). Tropical climate instability: The last glacial cycle from a Qinghai-Tibetan ice core. *Science*, *276*(5320), 1821–1825. https://doi.org/10.1126/science.276.5320.1821

Tofelde, S., Duesing, W., Schildgen, T. F., Wickert, A. D., Wittmann, H., Alonso, R. N., & Strecker, M. (2018). Effects of deep-seated versus shallow hillslope processes on cosmogenic ^{10}Be concentrations in fluvial sand and gravel. *Earth Surface Processes and Landforms*, *43*(15), 3086–3098. https://doi.org/10.1002/esp.4471

Uppala, S. M., Kållberg, P. W., Simmons, A. J., Andrae, U., Bechtold, V. D. C., Fiorino, M., et al. (2005). The ERA-40 re-analysis. *Quarterly Journal of the Royal Meteorological Society: A Journal of the Atmospheric Sciences, Applied Meteorology and Physical Oceanography*, *131*(612), 2961–3012. https://doi.org/10.1256/qj.04.176

Upreti, B. (1999). An overview of the stratigraphy and tectonics of the Nepal Himalaya. *Journal of Asian Earth Sciences*, *17*(5–6), 577–606. https://doi.org/10.1016/S1367-9120(99)00047-4

Valdiya, K. S. (1991). The Uttarkashi earthquake of 20 October: Implications and lessons. *Current Science*, *61*, 801–803.Retrieved from http://pascal-francis.inist.fr/vibad/index.php?action=getRecordDetail&idt=5222562

Van Der Beek, Van Melle, J., Guillot, S., Pêcher, A., Reiners, W., Nicolescu, S., & Latif, M. (2009). Eocene Tibetan plateau remnants preserved in the northwest Himalaya. *Nature Geoscience*, *2*(5), 364. https://doi.org/10.1038/ngeo503

Vance, D., Bickle, M., Ivy-Ochs, S., & Kubik, W. (2003). Erosion and exhumation in the Himalaya from cosmogenic isotope inventories of river sediments. *Earth and Planetary Science Letters*, *206*(3–4), 273–288. https://doi.org/10.1016/S0012-821X(02)01102-0

Vannay, C., Grasemann, B., Rahn, M., Frank, W., Carter, A., Baudraz, V., & Cosca, M. (2004). Miocene to Holocene exhumation of metamorphic crustal wedges in the NW Himalaya: Evidence for tectonic extrusion coupled to fluvial erosion. *Tectonics*, *23*, 1–24. https://doi.org/10.1029/2002TC001429

Von Blanckenburg, F. (2005). The control mechanisms of erosion and weathering at basin scale from cosmogenic nuclides in river sediment. *Earth and Planetary Science Letters*, *237*(3–4), 462–479. https://doi.org/10.1016/j.epsl.2005.06.030

Von Blanckenburg, F., Hewawasam, T., & Kubik, P. W. (2004). Cosmogenic nuclide evidence for low weathering and denudation in the wet, tropical highlands of Sri Lanka. *Journal of Geophysical Research*, *109*(F3), 1–22. https://doi.org/10.1029/2003JF000049

Wagnon, P., Linda, A., Arnaud, Y., Kumar, R., Sharma, P., & Vincent, C. (2007). Four years of mass balance on Chhota Shigri Glacier, Himachal Pradesh, India, a new benchmark glacier in the western Himalaya. *Journal of Glaciology*, *53*(183), 603–611. https://doi.org/10.3189/002214307784409306

Walia, M., Yang, T. F., Liu, T. K., Kumar, R., & Chung, L. (2008). Fission track dates of Mandi granite and adjacent tectonic units in Kulu–Beas valley, NW Himalaya, India. *Radiation Measurements*, *43*, S343–S347. https://doi.org/10.1016/j.radmeas.2008.04.040

Walker, J. D., Martin, M. W., Bowring, S. A., Searle, M., Waters, D. J., & Hodges, K. V. (1999). Metamorphism, melting, and extension: Age constraints from the High Himalayan slab of southeast Zanskar and northwest Lahaul. *The Journal of Geology*, *107*(4), 473–495. https://doi.org/10.1086/314360

Ward, D. J., & Anderson, R. S. (2011). The use of ablation-dominated medial moraines as samplers for ^{10}Be-derived erosion rates of glacier valley walls, Kichatna Mountains, AK. *Earth Surface Processes and Landforms*, *36*(4), 495–512. https://doi.org/10.1002/esp.2068

Watanabe, T., Dali, L., & Shiraiwa, T. (1998). Slope denudation and the supply of debris to cones in Langtang Himal, Central Nepal Himalaya. *Geomorphology*, *26*(1–3), 185–197. https://doi.org/10.1016/S0169-555X(98)00058-0

Weiers, S. (1995). On the climatology of the NW Karakorum and adjacent areas: Statistical analyzes including weather satellite images and a Geographical Information System (GIS). Bonn Geographical Society. In *Commission with F. Dümmler* (Vol. 92, p. 168).

Willenbring, J. K., Gasparini, N. M., Crosby, B. T., & Brocard, G. (2013). What does a mean mean? The temporal evolution of detrital cosmogenic denudation rates in a transient landscape. *Geology*, *41*(12), 1215–1218. https://doi.org/10.1130/G34746.1

Wittmann, H., Malusà, M. G., Resentini, A., Garzanti, E., & Niedermann, S. (2016). The cosmogenic record of mountain erosion transmitted across a foreland basin: Source-to-sink analysis of in situ 10Be, 26Al and 21Ne in sediment of the Po river catchment. *Earth and Planetary Science Letters*, *452*, 258–271. https://doi.org/10.1016/j.epsl.2016.07.017

Wobus, C. W., Hodges, K. V., & Whipple, K. X. (2003). Has focused denudation sustained active thrusting at the Himalayan topographic front? *Geology*, *31*(10), 861–864. https://doi.org/10.1130/G19730.1

Wulf, H., Bookhagen, B., & Scherler, D. (2010). Seasonal precipitation gradients and their impact on fluvial sediment flux in the Northwest Himalaya. *Geomorphology*, *118*(1–2), 13–21. https://doi.org/10.1016/j.geomorph.2009.12.003

Yanites, B. J., Tucker, G. E., & Anderson, R. S. (2009). Numerical and analytical models of cosmogenic radionuclide dynamics in landslide-dominated drainage basins. *Journal of Geophysical Research*, *114*(F1), 1–20. https://doi.org/10.1029/2008JF001088

Yin, A., & Harrison, T. M. (2000). Geologic evolution of the Himalayan-Tibetan orogen. *Annual Review of Earth and Planetary Sciences*, *28*(1), 211–280.

Zeitler, K., Koons, O., Bishop, M., Chamberlain, C., Craw, D., Edwards, M. A., et al. (2001). Crustal reworking at Nanga Parbat, Pakistan: Metamorphic consequences of thermal-mechanical coupling facilitated by erosion. *Tectonics*, *20*(5), 712–728. https://doi.org/10.1029/2000TC001243